

**Seismic Determination of Reservoir Heterogeneity: Application to the
Characterization of Heavy Oil Reservoirs**

Final Report

Report Period: 09/01/2000 - 08/31/2004

Matthias G. Imhof

February 2005

DE-FC26-00BC15301

Matthias G. Imhof

Department of Geosciences

Virginia Tech

4044 Derring Hall (0420)

Blacksburg, VA 24061

James W. Castle

Department of Geological Sciences

Clemson University

340 Brackett Hall

Clemson, SC 29634-0976

Disclaimer

This report was prepared as an account of work sponsored by an agency of the United States Government. Neither the United States Government nor any agency thereof, nor any of their employees, makes any warranty, express or implied, or assumes any legal liability or responsibility for the accuracy, completeness, or usefulness of any information, apparatus, product, or process disclosed, or represents that its use would not infringe privately owned rights. Reference herein to any specific commercial product, process, or service by trade name, trademark, manufacturer, or otherwise, does not necessarily constitute or imply its endorsement, recommendation, or favoring by the United States Government or any agency thereof. The views and opinions of authors expressed herein do not necessarily state or reflect those of the United States Government or any agency thereof.

Abstract

The objective of the project was to examine how seismic and geologic data can be used to improve characterization of small-scale heterogeneity and their parameterization in reservoir models. The study focused on West Coalinga Field in California.

The project initially attempted to build reservoir models based on different geologic and geophysical data independently using different tools, then to compare the results, and ultimately to integrate them all. Throughout the project, however, we learned that this strategy was impractical because the different data and model are complementary instead of competitive. For the complex Coalinga field, we found that a thorough understanding of the reservoir evolution through geologic times provides the necessary framework which ultimately allows integration of the different data and techniques.

Contents

Executive Summary	7
Cumulative Project Bibliography	8
Theses and Dissertations	8
Publications	8
Presentations and Extended Abstracts	9
1 Introduction	11
1.1 Motivation	11
1.2 Study Area	11
1.3 Organization of Study	15
2 Geologic Overview	17
2.1 Introduction	17
2.2 Tectonic Evolution of the San Joaquin Basin	19
2.3 Depositional History	21
2.4 Reservoir Architecture	21
2.5 Discussion	23
3 Wireline Correlations	25
3.1 Introduction	25
3.2 Cores and Wireline Logs	25
3.3 Depositional Environments	26
3.4 Core Correlations	27
3.5 Wireline Correlation	28
3.6 Discussion	32
4 Wireline-Based Heterogeneity Models	33

4.1	Introduction	33
4.2	Modeling Procedure	33
4.3	Modeling Results	35
4.4	Discussion and Conclusions	37
5	Seismic Heterogeneity	41
5.1	Introduction	41
5.2	Attribute Estimation	41
5.3	Discussion	45
6	Seismic Interpretation	49
6.1	Introduction	49
6.2	Seismostratigraphic Interpretation	49
6.3	Seismogeomorphic Interpretation	50
6.4	Discussion	52
7	Integration of Geologic Models and Seismic Data	58
7.1	Introduction	58
7.2	Integrated Heterogeneity Models	58
7.3	Model Comparisons	60
7.4	Comparison of Data Sets	62
7.5	Comparison of Modeling Methods	63
7.6	Discussion	63
8	Object-Based Stochastic Facies Inversion with Parameter Optimization	66
8.1	Introduction	66
8.2	Process	66
8.3	Application to the Coalinga Field	67
8.4	Discussion and Conclusions	70

9 Discussion 73

10 Bibliography 76

Executive Summary

The objective of the project was to examine how seismic data can be used to improve characterization of small-scale heterogeneity and their parameterization in reservoir models. Initially, we attempted to build independent reservoir models based on different geologic and geophysical data and different tools. Throughout the project, however, we learned that this strategy was impractical because the different data and model are complementary instead of competitive. The different methods and models require qualitative and quantitative information which can be obtained from others. Furthermore, we also experienced that the process was not strictly linear, but rather iterative. For example, the seismic interpretation in the traditional sense was the foundation of the project, but was also continuously updated and refined, and the results were used to segment and constrain other models.

For the complex Coalinga field, we found that a thorough understanding of the reservoir evolution through geologic times both conceptually and practically provided the framework which allowed integration of the different data and techniques. We built this framework by interpreting outcrops, cores, wireline, and seismic data. With this framework in place, we progressed through a sequence of heterogeneity models which started with simple wireline log interpolation, continued with geostatistical models based on wireline data and/or seismic data, and finally ended up with a modeling technique which truly integrated seismic and wireline data through a lengthy optimization process.

Cumulative Project Bibliography

Theses and Dissertations

K. L. Mize, ‘Development of Three-Dimensional Geological Modeling Methods using Cores and Geophysical Logs, West Coalinga Field, California’, MS Thesis, Clemson University, 2002.

J. L. Piver, ‘Integration of Geologic Models and Seismic Data to Characterize Interwell Heterogeneity of the Miocene Temblor Formation, Coalinga, California’, MS Thesis, Clemson University, 2004.

E. Nowak, ‘Applications of the Radon transform, Stratigraphic filtering and Objected-based Stochastic Reservoir Modeling’, PhD Dissertation, Virginia Tech, 2004.

S. Mahapatra ‘Deterministic High-Resolution Seismic Reservoir Characterization’, PhD Dissertation, Virginia Tech, in preparation.

Publications

M. G. Imhof, ‘Scale Dependence of Reflection and Transmission Coefficients’, *Geophysics*, 68(1), 322–336, 2003.

M. G. Imhof and W. Kempner, ‘Seismic Heterogeneity Cubes and Corresponding Equiprobable Simulations’, *Journal of Seismic Exploration*, 12(1), 1–16, 2003.

E. Nowak and M. G. Imhof, ‘Stratigraphic filtering’, *Geophysics*, submitted.

E. Nowak, M. G. Imhof, and W. Kempner, ‘Object-Based Stochastic Facies Inversion’, *Computers & Geosciences*, in preparation.

Presentations and Extended Abstracts

M. G. Imhof, 'The Heterogeneity Cube: a Family of Seismic Attributes', 71st Annual International Meeting of the Society of Exploration Geophysicists, San Antonio, 2001.

M. G. Imhof, 'The Heterogeneity Cube: a Family of Seismic Attributes', American Association of Petroleum Geologists Annual Convention, Houston, 2002.

M. G. Imhof, 'Estimation of 3D Reservoir Heterogeneity using Seismic Heterogeneity Cubes', 64th Meeting in Florence, European Association of Geoscientists & Engineers, Extended Abstracts, 2002.

E. Nowak, M. G. Imhof, and W. Kempner, 'Object-Based Stochastic Facies Inversion: Application to the Characterization of Fluvial Reservoirs', 72nd Annual International Meeting of the Society of Exploration Geophysicists, Salt Lake City, 2002.

K. L. Mize, J. W. Castle, F. J. Molz, and M. G. Imhof, 'Integration of Stratigraphy and Seismic Geophysics for Improved Resolution of Subsurface Heterogeneity', Clemson University Tenth Annual Hydrogeology Symposium Abstracts with Program, April 2002, p. 28.

J. L. Piver, J. W. Castle, M. T. Poole, R. A. Hodges, and M. G. Imhof, 'Integrating Geologic Models and Seismic Data to Characterize Interwell Heterogeneity of the Miocene Temblor Formation, Coalinga, California', Geological Society of America Abstracts with Programs, March 2003, v. 35, no. 1, p. 54.

J. L. Piver, J. W. Castle, M. T. Poole, R. A. Hodges, and M. G. Imhof, 'Characterization of Stratigraphic Heterogeneity in the Temblor Formation (Miocene), Coalinga Area, California: Integration of Geologic Models and Seismic Geophysical Data', Clemson University Eleventh Annual Hydrogeology Symposium Abstracts with Program, April 2003, p. 20.

M. G. Imhof and W. C. Kempner, 'Seismic Heterogeneity Cubes and Corresponding Equiprobable Simulations', American Association of Petroleum Geologists Annual Convention, Salt

Lake City, 2003.

S. Mahapatra, M. G. Imhof, and W. C. Kempner, 'Deterministic High-Resolution Seismic Reservoir Characterization', American Association of Petroleum Geologists Annual Convention, Salt Lake City, 2003.

M. G. Imhof, 'Equiprobable Simulations of Seismic Heterogeneity Cubes', 65th Meeting of the European Association of Geoscientists & Engineers, Stavanger, 2003.

M. G. Imhof, 'Seismic Heterogeneity Cubes and Corresponding Equiprobable Simulations', Interpreting Reservoir Architecture Using Scale-Frequency Phenomena, Oklahoma Geological Society and National Energy Technology Laboratory, Oklahoma City, 2003.

E. Nowak, M. G. Imhof, and W. Kempner, 'Object-Based Stochastic Facies Inversion', 73rd Annual International Meeting of the Society of Exploration Geophysicists, Dallas, 2003.

E. Nowak and M. G. Imhof, 'Stratigraphic Filtering', 73rd Annual International Meeting of the Society of Exploration Geophysicists, Dallas, 2003.

S. Mahapatra, M. G. Imhof, and W. Kempner, 'Poststack Interpretive Static Correction', 73rd Annual International Meeting of the Society of Exploration Geophysicists, Dallas, 2003.

J. Piver, J. W. Castle, M. T. Poole, R. A. Hodges, and M. G. Imhof, 'Integrating Geologic Models and Seismic Data to Characterize Interwell Heterogeneity of the Miocene Temblor Formation, Coalinga, California', Geological Society of America Joint Annual Meeting of the South-Central Section (37th) and Southeastern Section (52nd), Memphis, 2003.

E. Nowak and M. G. Imhof, 'Numerical Frequency Filtering in Binary Materials', 66th Meeting of the European Association of Geoscientists & Engineers, Paris, 2004.

S. Mahapatra, M. G. Imhof, and W. Kempner, 'Seismostratigraphic and seismogeomorphic reservoir characterization in Coalinga Field, California, U.S.', 74th Annual International Meeting of the Society of Exploration Geophysicists, Denver, 2004.

1 Introduction

1.1 Motivation

The objective of the study was to examine how different data can be used to parameterize models of short-scale reservoir heterogeneity. Short-scale heterogeneity has a controlling effect on reservoirs and fluid flow, yet they are not known at every point of interest in a deterministic manner because a particular feature may not intersect an outcrop, be penetrated by a well, or is insufficiently resolved on seismic data. Instead, short-scale heterogeneity is characterized by an often statistical model which allows their interpolation between outcrops and boreholes.

The original idea behind this study was first to compare many different methods to characterize and model reservoir heterogeneity based on geologic, wireline, and seismic data, and then to integrate the good results. Two years into the project, however, we realized that such an approach is rather impractical because the different methods and models are not completely independent. Instead, we changed from the hierarchical, rather tree-like structure (Figure 1(a)), to an approach where each model controls and constrains the next model. While this structure (Figure 1(b)) might have worked, it would also have sequentialized the entire project without opportunity to work in parallel, or to revise a model based on some later finding. Hence, the final structure of the project was semi-linear (Figure 1(c)) which allowed redoing an earlier step based on later findings. The key steps turned out to be geologic and seismic interpretation as their results provided the framework for the construction of the different heterogeneity models.

1.2 Study Area

The chosen study area was Coalinga field shown in Figure 2, a giant oil field in the San Joaquin valley of California with an extremely complex subsurface stratigraphy that has produced over 850 million barrels oil (MBO) of API gravity 20°. It is a mature oil field with

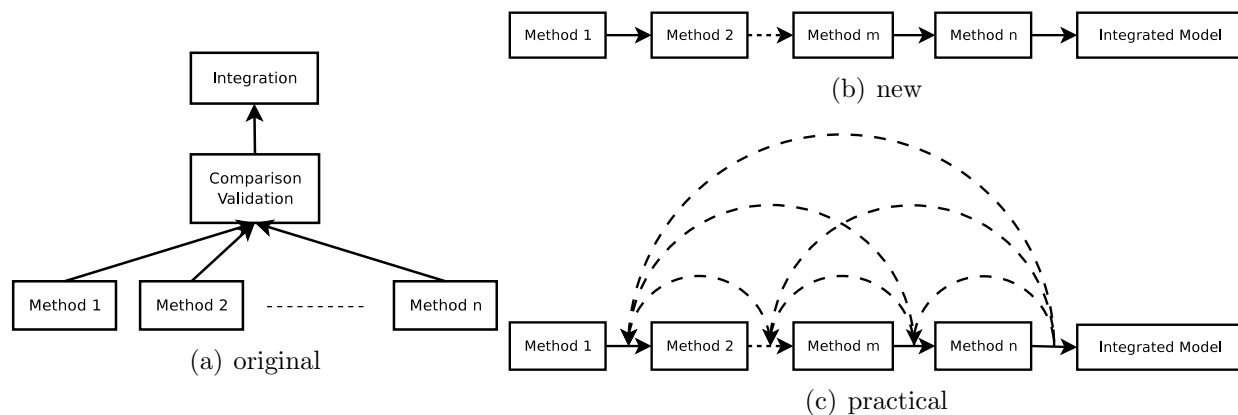


Figure 1: Project workflow: (a) the original plan called for independent heterogeneity models, a comparison, and late integration, (b) the new workflow allowed continuous integration, but in practice, (c) not every step could be finished in a perfectly sequential manner, and hence, later findings were incorporated by redoing earlier steps.

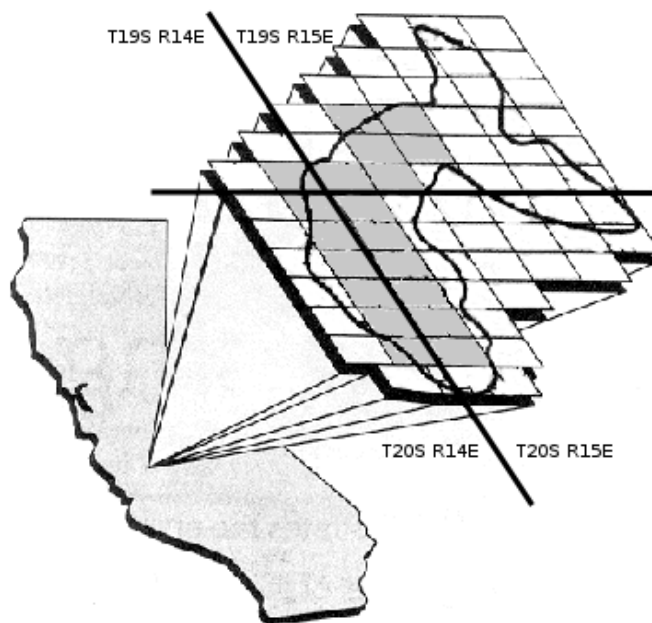


Figure 2: Location map of the Coalinga field in California. Each square block indicates a 1 sqmile area. The gray blocks are shown in more details in Figure 3.

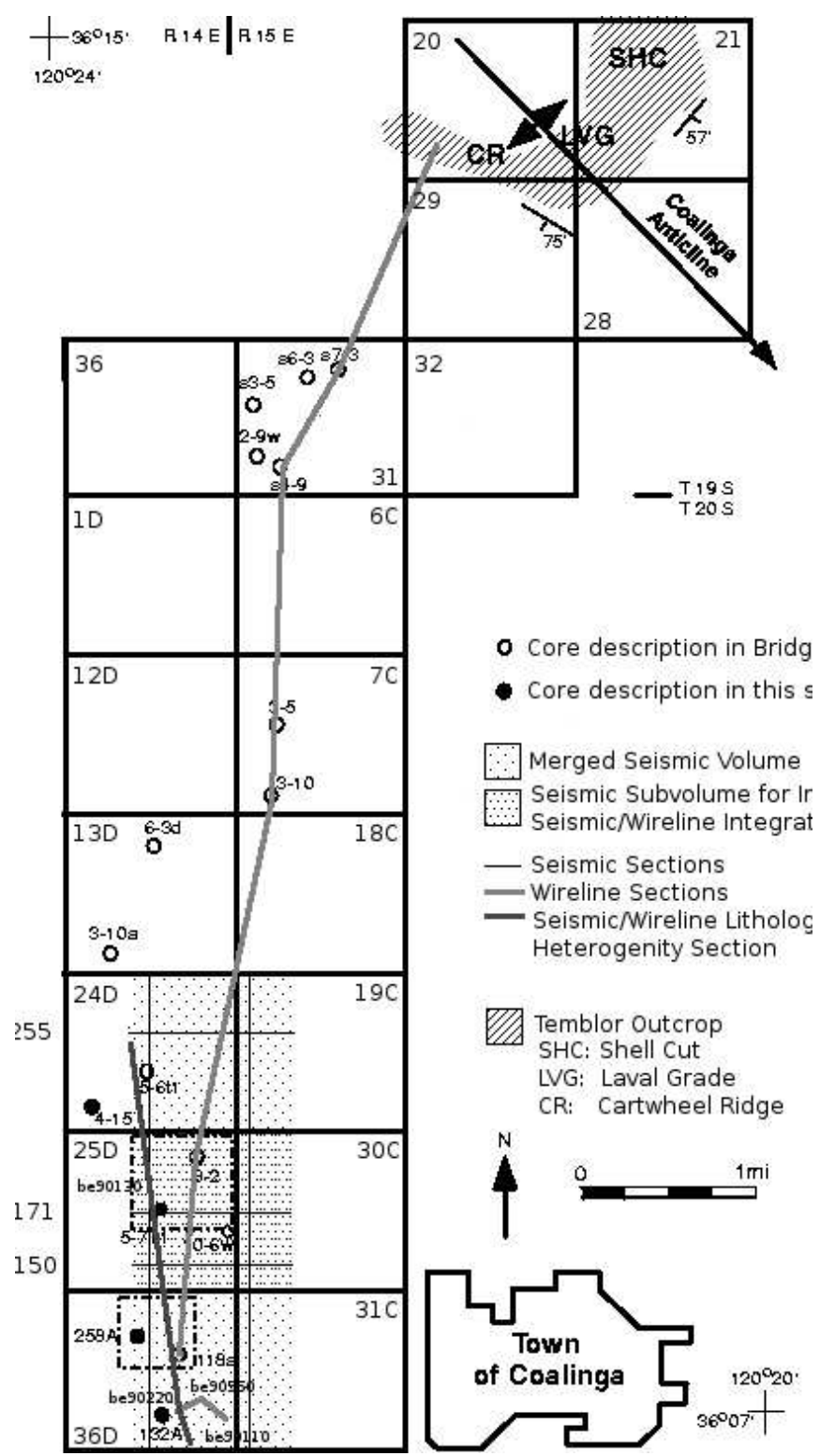


Figure 3: Location of the different focus areas, boreholes, and crosssections.

an abundance of core, wireline, and seismic data. The field has been oil and gas producing from the clastic Temblor formation (Miocene) since the early 1900's, and is now in its tertiary development stage. The Coalinga anticline is one of a series of echelon folds that modify the generally homoclinal eastern flank of the Diablo range along the west side of the San Joaquin Basin of California. The reservoir units are actually cropping out few miles to the north of the reservoir (Bridges and Castle, 2003).

The Coalinga field is divided into East Coalinga and West Coalinga (Figure 2) which influences production and distribution of producing wells. A northwest-southeast trending anticline (Coalinga nose) separates the two fields. The nose and its eastern part crosses regional strike and extends about five miles along the southeast plunge of the nose (Clark et al., 2001). Our focus, West Coalinga field, parallels the upturned, monoclinical west margin of the basin.

The field is part of the Kreyenhagen-Temblor petroleum system that derives oil from organic-rich shale of the Middle Eocene Kreyenhagen Formation as observed from the geochemical data analysis of the Kreyenhagen 74X-21H well (Peters et al., 1994). The reservoir trap is stratigraphic in nature. The reservoir rocks outcrop at the west margin where historical oil seeps and breaches were reported. The tight outcrops and solidified tar mats in the near surface of these outcrops provide the sealing mechanism (cap rocks) of the Temblor reservoirs. The accumulated heavy oil is produced by steam injection which fractionates the high-gravity oil beneath these sealants into low-gravity crude (Clark et al., 2001). At places, shales and calcite-cemented sandstone in the upper part of the Top Temblor create an effective top seal in the reservoir (Clark et al., 2001). The reservoir rocks are highly heterogeneous due to its proximity to the tectonically disturbed San Andreas transform.

The Temblor Formation sandstone contributes 90 percent of the total oil production as of 2001 (Clark et al., 2001). The average well depths range from 500 to 4500 ft. As of 2001, the total number of wells was 4000. The reservoir shows an average porosity of 0.34 and permeability ranging from 20 to 4000 md. The reservoir is about 700 ft thick in the east

margin of the field (down dip), but gradually thins towards west as it is truncated by the overlying Etchegoin Formation, which is a Pliocene oil producer. The reservoir rocks crop out along the west margin of the field. The oil seeps on the outcrops which were the pathfinder for the discovery of the field, ceased flowing as the field underwent development. Presently, about 2000 wells are under production by steam injection. About three to four barrels of steam are being pumped into the reservoir for every single barrel of oil recovery. The field requires more steam to be injected to produce oil than most other heavy oil reservoirs in the San Joaquin basin due to its geological complexities (Clark et al., 2001).

Hence, the reservoir complexity, the nearby outcrops, the number of wells with wireline and core data, and the availability of seismic data made this field the perfect area to build, compare, and integrate heterogeneity models.

1.3 Organization of Study

The study is presented in a strictly linear manner. As discussed earlier, many key results of the geologic and seismic interpretations were incorporated into the different heterogeneity models. These models were indeed used in a semi-linear fashion as many of their results guided the parameter selection for later ones.

Chapter 2 presents an overview over the regional geology and the architecture of Coalinga field. The overview is based on Bridges and Castle (2003) and Mahapatra (2005). Chapter 3 presents results obtained by analysis and correlation of wireline and core data based on Bridges and Castle (2003), Mize (2002), and Mahapatra (2005). Chapter 4 presents the first deterministic and stochastic heterogeneity models which were strictly based on wireline data. Mize (2002) focused on two areas in Sections 25D and 36D, each about a quarter square mile in extent (Figure 3). Chapter 5 presents heterogeneity models based only on seismic data (Imhof and Kempner, 2003) for the entire 3 square miles of the seismic coverage area (Figure 3). No considerations were given to facies tracts or unconformities. The results were estimate of variogram lags or correlation lengths which were later used in other parts of

the project for stochastic modeling. Chapter 6 presents the findings of seismostratigraphic and seismogeomorphic analyses (Mahapatra, 2005). The first key results were maps tracing the unconformities between wells over the entire seismic coverage area (Figure 3). The other key result was the observation that two seismofacies bodies collocated with good reservoir sands in the subtidal and incised-valley-fill tracts. In Chapter 7, we present heterogeneity models which are compatible both with wireline and seismic data (Piver, 2004). The models cover the central square mile of the total seismic coverage area for the project. Chapter 8 optimizes the integrated heterogeneity models for the entire seismic coverage area. Even with unreasonable geometry parameters, one can find realizations which are compatible with wireline and seismic data. Nowak (2004) derived an algorithm which not only finds compatible realizations, but also tweaks the model parameters to find the best ones. Chapter 9 finally wraps the study up with conclusions and a discussion.

2 Geologic Overview

2.1 Introduction

The San Joaquin basin is a strike-slip basin, and hence shows complex tectonics (Bridges and Castle, 2003). Both structural styles and the sedimentary geometries vary spatially very rapidly. The basin is located in the southern part of the 700 km long Great Valley of California in the vicinity of the San Andreas fault. The basin is an asymmetric structural trough with a broad, gently inclined eastern flank and a relatively narrow western flank which becomes a steep homocline in the northern part of the valley. In the southern part, it turns into a belt of folds and faults instead. The basin trough contains Upper Mesozoic to Cenozoic sediments which reach over 9 km thickness in the west-central part of the valley and at its southern end (Bartow, 1991). Bartow believes that the basin was a fore-arc basin which was mostly open to the Pacific Ocean on the west during late Mesozoic and early Cenozoic periods. During the late Cenozoic, the basin was converted into a transform-margin basin. The sediments were deposited on a westward tilted basement of Sierra Nevada plutonic, mafic, ultramafics, and metamorphic rocks of Jurassic age (Cady, 1975; Page, 1981). Bailey et al. (1964) propose that towards the west of the valley, both Mesozoic and early Tertiary Great Valley sequences along with the underlying ophiolite sequences are juxtaposed with the Franciscan Complex along a the Coast Range thrust (Figure 4). The basin is separated from the Sacramento basin to the north by the buried Stockton arch and Stockton fault (Figure 4). To the south, the basin is separated from the Maricopa-Tejon sub basin by the buried Bakersfield arch. Bartow (1991) observed that the Cenozoic strata in the San Joaquin basin thicken southeastwards from about 800 m in the north (western part of the Stockton arch) to over 9,000 m in the south (in the Maricopa-Tejon sub basin in the south). He also observed that the Mesozoic and early Tertiary Great Valley sequence thins out southeastward and is absent at the Bakersfield arch. Both arches had no appreciable structural relief but could contribute to this huge sedimentation during Cenozoic period due

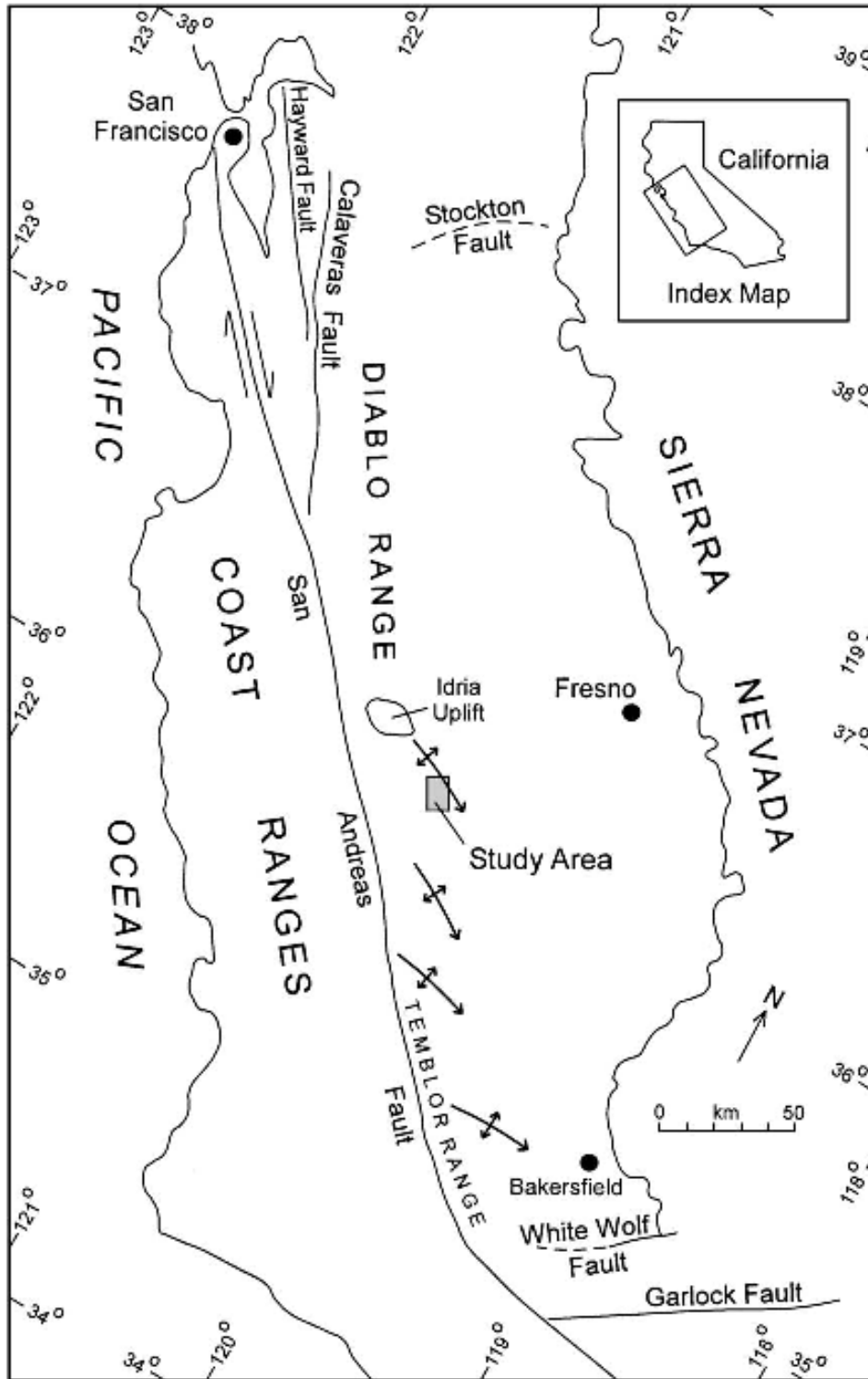


Figure 4: Regional overview of the tectonic elements around Coalinga field (Bridges and Castle, 2003).

to basin tilting phenomena associated with regional thrusting and plate kinematics. The Tertiary depocenters of these basins coincide with the depocenters of the Pleistocene and Holocene basins (Buena Vista and Kern Lakes basins to the south and the Tulare Lake basin in the central part) of the Valley (Bartow, 1991).

The San Joaquin basin shows discrete geomorphic and structural styles similar to that of the western Cordilleras, but the geology is inherently variable in stratigraphy and structural styles of deformation due to various Cenozoic intermittent uplifts and subsidence associated with the evolution of the Valley (Bartow, 1991). The Neogene sediments mostly consist of a thick marine section in the southern part and a thin non-marine section in the northern part of the basin. In addition, from a structure point of view, there exists a complex folded system in the western side of the basin while the eastern side has a little deformed sedimentary due to differential tectonic process which caused a north-south tilting and a western uplift of the valley.

2.2 Tectonic Evolution of the San Joaquin Basin

Sedimentation in the San Joaquin basin is mainly governed by tectonism, and to a lesser extent, by eustatic sea level changes and allocyclic factors like climate (Bartow, 1991). As a whole, the sedimentary record depicts the complex interplay of all of these factors. Thick sediments in the southern San Joaquin basin indicate the effect of tectonic subsidence. Moreover, the location of the basin along an active continental margin generated prolonged tectonic activity during the Cenozoic. Most of the marine sequences are unconformity bounded and are easy to correlate within the basin. In a few cases, the equivalent non-marine sequence may be correlated based on the position of the bounding surfaces.

Plate movements greatly influenced the tectonics and hence the evolution of the basin. A subduction zone has prevailed at the western margin of North America during Cenozoic times when the oceanic Kula plate subducted obliquely under the North American plate (Page and Engebretson, 1984). Bartow (1991) proposed that the rapid rate of convergence might have

made this subduction zone to be of low angle. The fast convergence rate is also observed by the presence of relatively displaced arc magmatism eastward from the Sierra Nevada into Colorado (Lipman et al., 1972; Cross and Pilger, 1978). This oblique subduction at the central California margin continued until end of the Eocene when the Farallon plate displaced the Kula plate (Page and Engebretson, 1984). A decrease in convergence rates in the late Eocene-Oligocene periods steepened the subduction zone and the volcanism, associated with the subduction process, migrated southwestward from Idaho and Montana into Nevada (Lipman et al., 1972; Cross and Pilger, 1978).

Beside global plate tectonics, there were regional tectonic events influenced the evolution of the San Joaquin basin (Bartow, 1991). A clockwise rotation of the southernmost Sierra Nevada produced large en echelon folds in the southern Diablo Range related to Late Cretaceous and early Tertiary right-lateral strike-slip movement on the proto-San Andreas fault (Harding, 1976; McWilliams and Li, 1985). Twisting and wrenching along the plate boundary resulted in the formation of a series of ridges and basins along the California coast (Bartow, 1991). Transgression and regression took place in the basins due to this tectonic force which caused the basins to rise and subside periodically. Also, large volume of sediments from the ridges were deposited in fluctuating depositional environments - from deep, offshore marine to shallow, near shore marine, and even erosional surfaces as the basin floor must have risen above the surface of the ocean at different times. The uplift of the Stockton arch in the early Tertiary, for example, served as a provenance for the Cenozoic sediments (Hoffman, 1964). In the Neogene, the wrench tectonism gave also rise to a series of en echelon folds, which deformed the San Joaquin Miocene deposits into a series of anticlines and synclines. Evidence for synsedimentary deformation is reflected in the distribution, facies and sedimentary packaging of strata due to the presence of local unconformities within the Temblor formation (Graham, 1985).

2.3 Depositional History

The San Joaquin basin was formed at the end of the Mesozoic on the southern part of an extensive forearc basin associated with the subduction of the Farallon plate under the North American plate. During the Cenozoic, the basin was gradually transformed into the present day hybrid intermontane basin. The geologic processes comprised a gradual restriction of the marine influx to the basin due to uplift of the northern part of the basin in the late Paleogene period. In the Neogene period, the marine influx towards the westside of the basin was partially cut off due to uplift of the Diablo and the Temblor Ranges (Harding, 1976; Bartow, 1991). During late Neogene and Quaternary, fluvial to lacustrine sediments were deposited in the basin (Marchand and Allwardt, 1981).

2.4 Reservoir Architecture

The Temblor Formation represents the interplay of shallow marine and non-marine depositional environments. The clastic shallow, unconsolidated reservoir is very heterogeneous in nature, as it is mostly bounded by unconformities. Outcrop and well data analysis identifies the Temblor Formation as an upward deepening depositional succession. Geological studies of outcrops, cores and gamma ray log (Bridges and Castle, 2003) showed that the reservoir is subdivided into three distinct depositional environments representing a near-shore fluvial dynamic depositional setting intermingled with depositional erosional hiatuses. The Temblor formation (lower to middle Miocene) overlies the Kreyenhagen crystalline clastics of Eocene. The base of the Temblor is formed by an unconformity (Base Temblor) representing a time period of 21 million years of non-deposition and aerial exposure (Bate, 1984; Bartow, 1991). The Base Temblor unconformity is considered equivalent to the bounding surface 1 (BS-1) of Bridges and Castle's (2003) classification (Table 3). This regionally extensive base unconformity was the result of a low relative regional sea level (lowstand) in the basin due to tectonic uplift (Bridges and Castle, 2003). The top of the Temblor is demarcated by a regional angu-

lar conformity (Top Temblor) equivalent to BS-6 (Table 3). The Santa Margarita Formation (upper Miocene) overlies the Temblor in the north. To the south, the Etchegoin formation (Pliocene) overlies this unconformity because the Santa Margarita Formation was eroded out. The Top Temblor unconformity represents a period of 5 million years of non-deposition and erosion (Bate, 1984; Bloch, 1999) caused by the tectonic uplift of Diablo Range (Harding, 1976; Bate, 1985). Based on litho-stratigraphic correlation and facies tract analysis, a regional unconformity (Button unconformity) demarcates the reservoir facies deposited on top of the Base temblor. This unconformity is equivalent to BS-3 (Table 3), a transgressive depositional lag with a base of Oyster bed which separates the shoreline facies ‘Button Beds’ (Bridges and Castle, 2003) from the underlying lowstand and estuarine facies. The reservoir on top of the Button unconformity is overlain by the Valv unconformity identified by the presence of a diatomite bed right underneath (BS-5). The Valv unconformity was formed as a response to uplift caused by the beginning of rapid movement along the San Andreas Fault.

The surfaces BS-2 and BS-4 of Bridges and Castle (2003) are based on the facies changes observed in the sedimentological analysis of cores, outcrops, and the presence of barnacle shells there in. The formation thickness bounded by these surfaces are relatively thinner and are not being considered for the present seismic analysis as it is difficult to map these thin sequences on the seismic data. Current (2001) identified eight lithofacies in the Temblor Formation based on core and out crop analysis. These are Sand, Burrowed Sand, Laminated Sand, Silt and Clay, Fossiliferous Sand and Clay, Burrowed Clay, Limestone, and Calcemented Sediment. Bridges and Castle (2003) carried out extensive analyses of cores and outcrops around Coalinga field and formulated five facies tracts. They attributed relative rise in sea levels caused by basin subsidence during the Temblor deposition to the occurrence of these facies tracts and attributed the cause of subsidence to the regional tectonic extension related to strike-slip movement associated with the San Andreas transform. The incised valley fill (IVF) facies tract was deposited on the Base Temblor unconformity on inci-

sions into the Kreyenhagen Shale during the lowstand period. This tract was overlain by an estuarine facies caused by local subsidence and rapid sedimentation. The basin then experienced deposition of tide- to wave-dominated progradational facies on top of the Buttonbed unconformity probably due to the uplift of the Diablo Range (Hoots et al., 1954) and the associated relative sea level changes on the east side of the San Joaquin basin (bloch, 1999). Diatomite were deposited above the tide to wave facies in brackish to shallow marine environments as a result of relative sea level fall (Bridges and Castle, 2003), which was capped by the Valv unconformity at a later stage. Subtidal deposits that occurred due to a subsequent rise in sea level overlie the diatomite facies tract. The zone is also bioturbated. Finally, the Temblor Formation was capped by the Top Temblor unconformity (BS-6) which separates the overlying Santa Margarita and Etchegoin formations on a regional scale (Bate, 1984; Bartow, 1991). Table 2 will list the various facies tracts present in the Temblor Formation and their characteristic features.

The four unconformities (Base Temblor, Buttonbed, Valv, and Top Temblor in ascending order) described above play significant roles in the distribution and flow of fluids in the reservoir. The changes associated with the above facies tracts render the reservoir highly heterogeneous and highly variable in porosity and permeability distribution. The thicknesses between the three facies tracts within the Temblor Formation vary over the field due to the presence of dynamic paleo-topography of the basin caused by varying degrees of tectonic uplift and differential amounts of sedimentation through out the period of deposition and erosion.

2.5 Discussion

The preceding overview on the role and effect of various geologic processes that shaped up the evolution of the San Joaquin basin from Cenozoic to Neogene clearly indicates the structural, sedimentological and depositional complexities that the basin had experienced in the geological past. The evolution of the Coalinga reservoir was influenced by plate

movement and its proximity to the San Andreas fault which caused subsidence and uplift. In combination with global sea level changes, the result is a very complex geology as evidenced in Coalinga field where intertwined tectonics and stratigraphy produce a highly heterogeneous and compartmentalized reservoir.

3 Wireline Correlations

3.1 Introduction

The field operator, ChevronTexaco, supplied wireline log data for over one hundred wells within the study areas and granted access to four additional cores for use in this study (Mize, 2002). These data allowed us to validate and refine the lithofacies groups defined by Bridges (2001). We also used the wireline data for construction of depth-structure contour maps which allow correlation of the seismic data with well data, and hence, the establishment of time-to-depth conversions and seismic well ties.

3.2 Cores and Wireline Logs

Fourteen lithofacies were identified in core, which were subsequently arranged into 7 lithofacies groups by similarities in grain size, degree of bioturbation, degree of cementation, sedimentary structures, and sorting (Table 1). The sand lithofacies group (1) is characterized by values of 0 to 30% on the scaled gamma ray log. The scaled gamma ray signature for this lithofacies group is relatively consistent with small variability. The log signature of the thinly laminated sand, silt, and clay lithofacies group (2) is highly variable with values between 20 and 75%. The scaled gamma ray spikes within the thinly laminated sections are thin in comparison to other spikes. The burrowed clay lithofacies group (3) ranges from 30 to 50% scaled gamma ray and contains one to three consistent spikes with a smooth, not irregular, signature. The burrowed sand lithofacies group (4) has a highly variable (irregular) log signature with several small spikes, and typically ranges from 10 to 40% scaled gamma ray, with scaled gamma ray values near the top of the Temblor ranging from 70 to 100%. Fossiliferous sand and clays (5) are characterized by their location just above the base of the Temblor Formation and consist of a large spike (70 to 100%) capped by a smaller spike in scaled gamma ray value. The limestone lithofacies group (6) occurs generally at the base of the Temblor and has a thickness of 3 to 6 ft. A spike in the density log and a low value

Lithofacies Group	Lithofacies	Environment
sand (1)	clean sand crossbedded sand pebbly sand	barrier/bar tidal flat, tidal bars or scour surfaces
thinly laminated sand, silt and clay (2)	clay and silt interlaminated sand and clay sandy clay	wavedominated offshore
burrowed clay (3)	burrowed clay	tidal flat
burrowed sand (4)	burrowed sand	barrier/bar tidal flat tidal bars or subtidal
fossiliferous sand and clay (5)	fossiliferous sand fossiliferous clay	lagoon low energy interval
limestone (6)	fossiliferous limestone	low energy interval marine flooding
calcareous cemented Sand (7)	cemented Sand calcareous Pebbly sand	scour surface lag diagenetic processes

Table 1: Lithofacies groups defined by similarities in grain size, degree of bioturbation, degree of cementation, sedimentary structures, and sorting.

in scaled gamma ray are characteristic of the limestone. The carbonate-cemented sands (7) are generally found at the top estuarine and top tide- to wave-dominated shoreline surfaces based on core. Scaled gamma ray values range up to 50%, with a scaled gamma ray spike and common resistivity and density kicks.

3.3 Depositional Environments

Based on the core descriptions, three depositional environments are interpreted for the Temblor Formation in the southern part of West Coalinga Field: (1) estuarine; (2) tide- to wave-dominated shoreline; (3) and subtidal (Mize, 2002) The incised valley deposits interpreted by Bridges (2001) and Bridges and Castle (2003) as occurring below the estuarine interval north of the present study area were not observed in core from the southern portion of the field. They also described a separate facies tract between the tide- to wave- dominated shoreline and subtidal facies tracts. This diatomite facies tract consists of diatomaceous clay

Well Num.	132A	258A	5-7T1	4-15
Identifier	IR85310	IO06270	IN50250	IO95320
Section	36D	36D	25D	24D
subtidal	abundant horizontal to vertical burrow structures, rare thin clay and limestone beds, mottled appearance	abundant horizontal to vertical burrow structures, rare thin clay beds and calcareous intervals, mottled appearance	abundant horizontal to vertical burrow structures, rare thin clay beds, mottled appearance	abundant horizontal to vertical burrow structures, rare thin clay beds, mottled appearance
tide- to wave-dominated shoreline	minor fining upward sequences (4-8 ft), minor coarsening upward sequence (3-6 ft), abundant low angle planar cross-bedding, rare ripple cross-lamination, minor clay drapes, rare lag beds with common mud rip-ups and pebbles, faint parallel bedding, abundant burrow structures	common fining upward sequences (3-6 ft), minor coarsening upward sequences (3-20 ft), rare low angle planar cross bedding, rare lag beds with mud rip-ups, common burrow structures	minor coarsening upward sequences (3-6 ft), rare low angle planar cross-bedding, rare ripple cross-lamination, minor clay drapes, rare lag beds with common mud rip-ups and pebbles, rare faint parallel bedding, abundant burrow structures	minor fining upward sequences (2-6 ft), rare coarsening upward sequences (2-5 ft), rare to common low angle planar cross-bedding, rare ripple cross-lamination, minor clay drapes, rare lag beds with common mud rip-ups and pebbles, rare faint parallel bedding, common burrow structures
estuarine	rare fining upward sequences, common scour surfaces with mud rip-ups and pebbles, rare ripple cross-laminations, common to abundant tabular cross bedding, rare to common clay drapes, rare flaser bedding, abundant shell fragments (clay and sand near base Temblor), rare coarsening upward sequences, rare burrow structures	rare fining upward sequences, rare scour surfaces with mud rip-ups and pebbles, abundant shell fragments (clay and sand near base Temblor), rare large coarsening upward sequences, rare to common burrow structures	rare fining upward sequences, common scour surfaces with mud rip-ups and pebbles, rare ripple cross-laminations, common tabular cross bedding, rare clay drapes, Abundant shell fragments (clay and sand near base Temblor), Rare coarsening upward sequences, common burrow structures	common fining upward sequences, common scour surfaces with mud rip-ups, rare tabular cross bedding, rare clay drapes, abundant shell fragments (clay and sand near base Temblor), abundant burrow structures

Table 2: Physical and biological features of depositional environment intervals.

which grades laterally into burrowed clay towards the southern end of the field. In the northern part of the section 25D study area, thin (3 to 10 feet thick) burrowed clays beds occur immediately below the subtidal lithofacies group. These burrowed clay beds were not separated into a separate depositional environment due to the lack of spatial coverage of the burrowed clays within logs and cores.

3.4 Core Correlations

Core descriptions were compared with gamma ray and density logs to identify the following bounding surfaces for modeling purposes: base Temblor, clay concentration, top estuarine, top tide- to wave-dominated shoreline, and top Temblor (Figure 5(a)). The base Temblor surface occurs below a thick (70 to 100 ft) coarsening upward sequence and coincides with a spike in the density log, which is also just below a decrease in gamma ray values. This density spike is correlative with the limestone found at the base of the Temblor Formation. The clay concentration surface is placed at the inflection point above a clay concentration at

Location	Environment	Geologic Bounding Surface	Seismic Unconformity
Top Temblor	Top Subtidal	BS 6	Top Temblor
Top Diatomite / Burrowed Clay	Transitional	BS 5	Valv
Top Tidal Wave Dominated	Top Tidal Wave Dominated	BS 4	Not detected
Top Estuarine	Top Estuarine	BS 3	Buttonbed
Clay Concentration	Top Incised Valley Fill	BS 2	Not detected
Base Temblor	Bottom Incised Valley Fill	BS 1	Base Temblor

Table 3: Relationships between environments, geologic bounding surfaces, and seismic unconformities.

the top of a large fining upward sequence on the scaled gamma ray log. The top estuarine surface corresponds to the inflection point on the top of a large gamma kick at the top of a fining upward sequence, which dominates the upper part of the estuarine interval. The top of the tide- to wave-dominated shoreline surface is at the lower inflection point of a large gamma spike at the base of a coarsening upward sequence of the subtidal interval. This spike generally is the highest gamma ray value within the Temblor Formation, with few exceptions. The subtidal zone has two sets of large gamma spikes (Figure 5(a); elevation of -710 to -730 ft and -683 to -705 ft). The top Temblor surface is placed above these two sets at the top inflection point of a coarsening upward sequence.

Not all bounding surfaces described by Bridges and Castle (2003) can be detected seismically. The nomenclature for the seismic unconformities follows Clark et al. (2001). The relations between geologic bounding surfaces and seismic unconformities are listed in Table 3. Figure 6 presents a schematic crosssection based on core descriptions illustrating the stratigraphic relationships of bounding surfaces, environments, facies tracts, and lithologies.

3.5 Wireline Correlation

In order to integrate geologic with seismic data, we correlated sonic and density logs from wells within the seismic coverage area to identify and trace the four unconformities which are observable seismically (Table 3. Figure 5(b) shows the seismic unconformities pasted onto

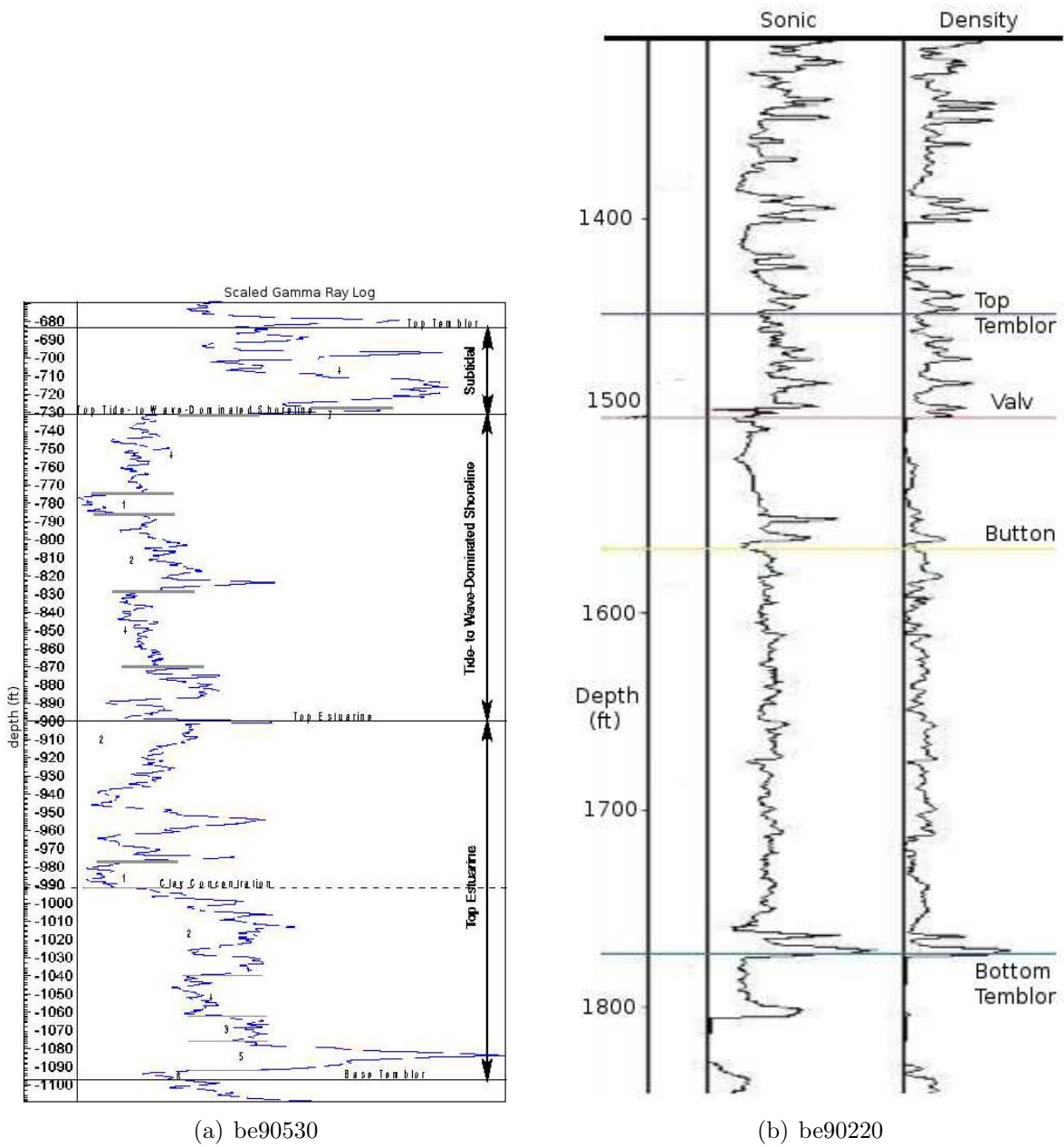


Figure 5: Wells be90530 and be90220 in Section 25D: Depositional environments, geologic bounding surfaces, and lithofacies groups listed by number for well be90530. Seismic unconformities are marked on well be90220.

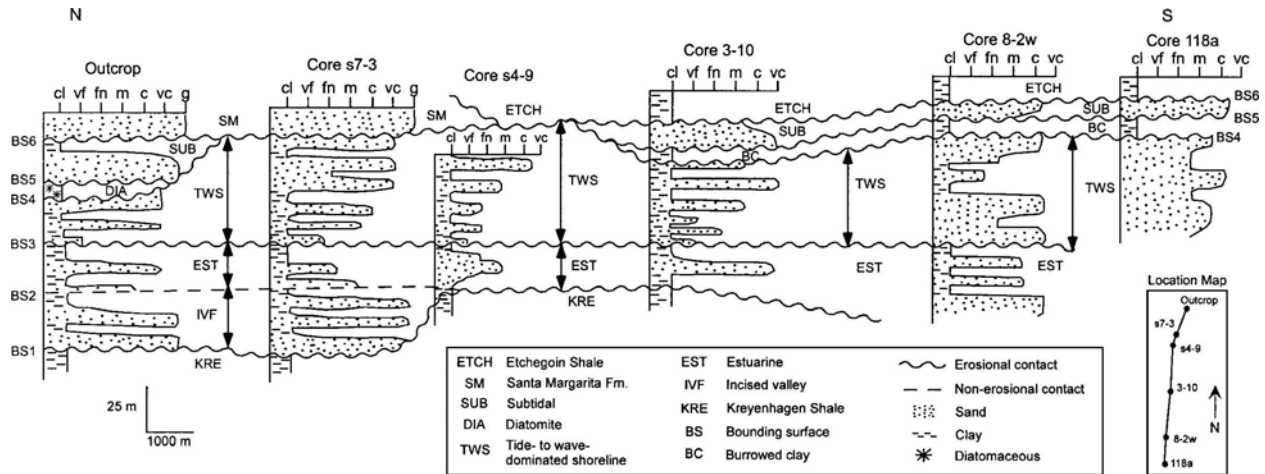
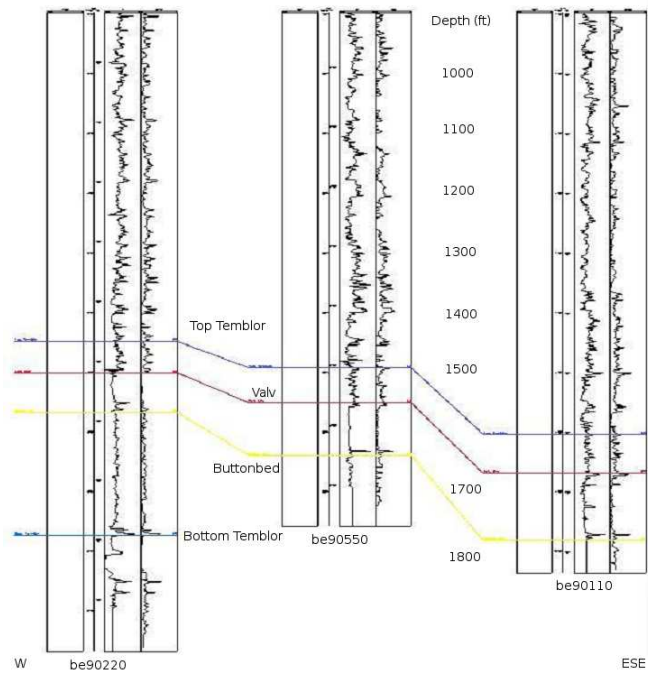
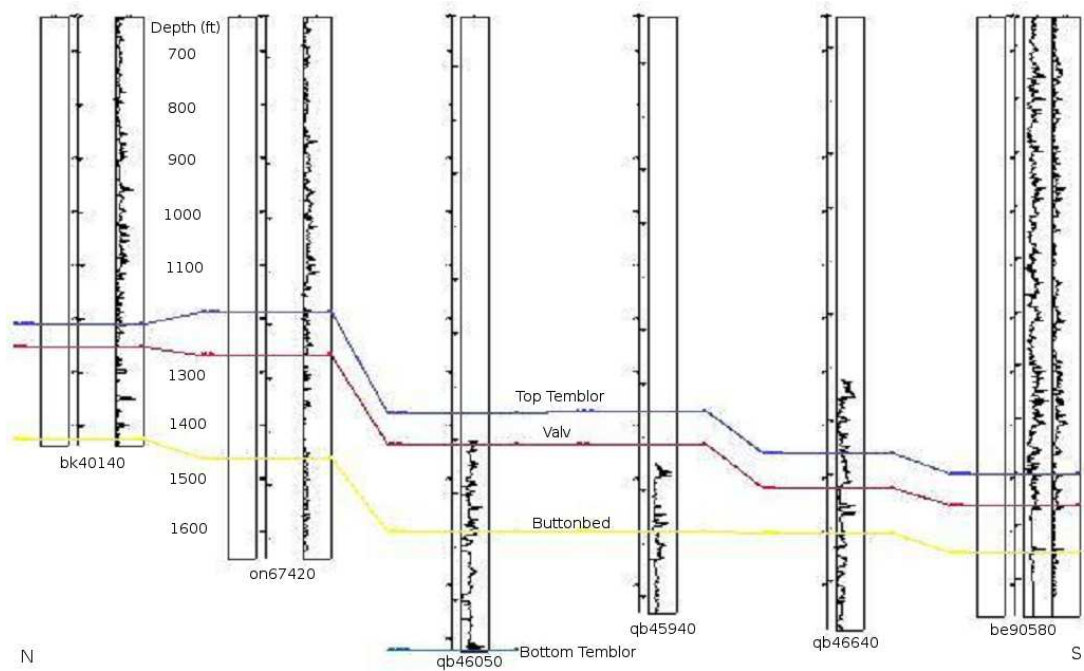


Figure 6: A schematic crosssection based on core descriptions showing the stratigraphic relationships between bounding surfaces and facies tracts (after Bridges and Castle, 2003).

the density and sonic logs of well be90220. These picks were then correlated between wells to generate wireline crosssections. The crosssections show that the reservoir rocks exhibit vertical variations in formation thickness and degree of sediment compaction. Shifting of the shale base lines is observed with respect to each unconformity bounded formation. When exact picking of the unconformities was difficult on density and sonic logs, we worked with the neutron porosity logs as variation in compaction factor also affects the porosity values. We were able to identify the four unconformable surfaces (Base Temblor, Buttonbed, Valv, and Top Temblor) based on the shale base trend line shifting (Figure 7). The wireline-based depth picks for the unconformities were interpolated to generate structure and isopach maps for the different facies tracts. Figure 8 shows the depth structure contours and isopachs for the entire Temblor interval. The generic strike of the Temblor seems to be in the NNE-SSW direction. The Temblor top is shallowest towards the southwestern corner of the seismic coverage area. The thickness of the Temblor formation is increasing downdip towards east in the northeastern corner of the seismic coverage area.



(b) W-ESE

Figure 7: Wireline crosssections with correlated unconformities.

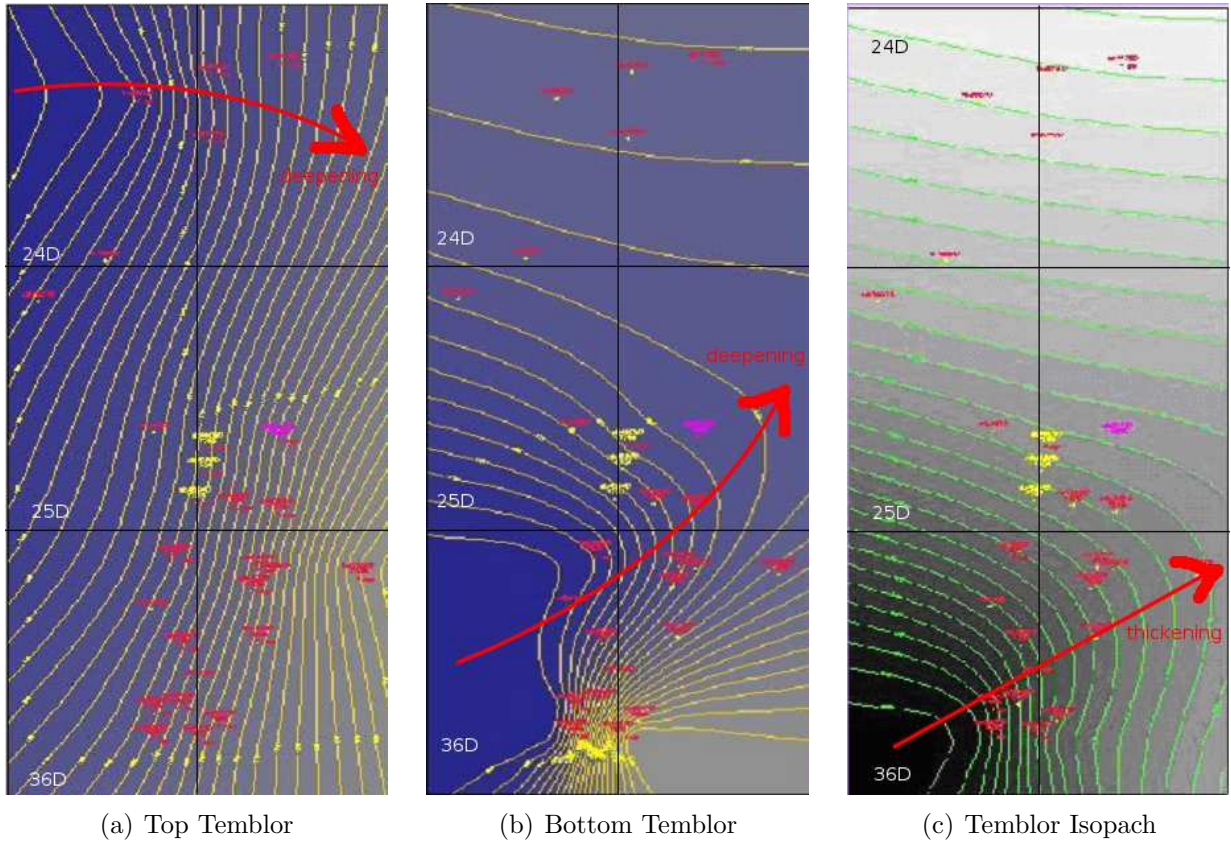


Figure 8: Wireline crosssections with correlated unconformities.

3.6 Discussion

We used outcrop data, cores, and wireline logs to define a structural and stratigraphic framework including facies tracts and bounding surfaces. This framework enables us to correlate seismic unconformities to geologic bounding surfaces. Furthermore, the framework establishes at the conversion of seismic time to wireline depth.

4 Wireline-Based Heterogeneity Models

4.1 Introduction

Two areas with extents of roughly a quarter square mile ($\approx 0.6 \text{ km}^2$) were chosen for intensive analyses of cores and wireline data. One area is in the north-central portion of section 36D and contains 28 wells. The other area is located in the northeast portion of section 25D and contains 66 wells. They were chosen based on their well and 3-D seismic coverage. The analyses results were used for construction of four types of 3-D heterogeneity models: deterministic, stochastic lithofacies, stochastic petrophysics, and conditioned (Mize, 2002).

4.2 Modeling Procedure

Because the wireline logs were of different vintages, we decided to normalize the natural gamma logs. The minimum value was determined by locating the minimum value for a given gamma-ray log within the interpreted Temblor Formation. The maximum value was the highest gamma value within the Temblor Formation, which occurs most often at the base of the subtidal environment. Structure contour maps were created in RMS (RMS, 2002) for each of the four bounding surfaces: base Temblor, top estuarine, top tide- to wave-dominated shoreline, and top Temblor. Even though it is not a structural bounding surface, a contour map was also created for the clay concentration surface in each section because it is used for stochastic, deterministic, and conditioned models. The surfaces generally have the same attitude, dipping towards the east-southeast, though this general dip most likely is the result of post-depositional tectonics.

The contour and corresponding isopach maps were used to generate realizations using four different techniques: (1) deterministic, (2) stochastic, (3) petrophysical, and (4) conditioned reservoir modeling.

Deterministic models refer to those that use only continuous well data and distribute well properties throughout the model using Kriging algorithm to produce a single realization

(Isaaks and Srivastava, 1989). Deterministic models were created for the scaled gamma ray logs in both study areas. Influence radii of 900 ft in the X and Y directions were used for section 25D, and 25 ft in the Z direction for the estuarine and tide- to wave-dominated shoreline intervals while the subtidal required an influence radius of 800 ft in the X and Y directions, and 20 ft in the Z direction. Influence radii of 1000 ft (X and Y directions) and 75 ft (Z direction) were used in the estuarine and tide- to wave-dominated shoreline for section 36D. The larger Z direction influence radii were used in section 36D to enable the software to interpolate the entire model between the data points. The subtidal zone model was created with an X and Y influence radii of 650 ft and a Z influence radius of 25 ft. The influence radii were established so that the model would be interpolated for all areas not covered by wells.

Stochastic models retain the ability to produce equally probable realizations of subsurface heterogeneity. Two types of stochastic models were created: lithofacies models and petrophysical models. Lithofacies models use upscaled discrete logs (lithofacies groups), and represent the distribution of the different lithofacies types in each zone. A lithofacies model illustrates the spatial relationships among lithofacies bodies and is required before petrophysical or conditioned models can be created.

Petrophysical modeling is used to produce models of a parameter (for example, scaled gamma ray, porosity, permeability, etc.) according to a chosen stochastic lithofacies model using the upscaled well data and lithofacies group parameters. Petrophysical modeling uses the results from lithofacies modeling and produces a set of probabilistic outcomes of parameter distribution (scaled gamma ray in this case) that can be compared in order to evaluate the uncertainty associated with the reservoir description. The two steps involved in creating a petrophysical stochastic model are defining the model job, which establishes the premises for the stochastic simulation, and performing the simulation to obtain the modeling results. Defining the model job involves transforming the scaled gamma ray data into a Gaussian or normal distribution for each zone. After transformations are performed, variograms are

created.

Conditioned reservoir models are models in which continuous scaled gamma ray data is interpolated by a weighted moving average for each body modeled in the stochastic lithofacies model. By creating a conditioned model, both the discrete and continuous data are incorporated into the model. Conditioned models are built by creating a stochastic lithofacies model and deterministically modeling the scaled gamma ray data for each body of the stochastic lithofacies realization.

4.3 Modeling Results

Important differences in resolution and accuracy were observed among the four types of models. These results are summarized in Table 4. Examples of the models are shown in Figures 3 through 10. The tide- to wave-dominated shoreline interval on the deterministic, petrophysical, and conditioned models has a similar appearance, but the petrophysical and conditioned models are the most similar. There are only a few slight differences at the top of the interval. The estuarine interval of the petrophysical model has scaled gamma ray values that are much lower than those of both the deterministic and conditioned models, which is likely due to the transformation of scaled gamma ray values using the variograms. No major differences are apparent in the subtidal interval of the conditioned model and deterministic models. The estuarine interval is also similar in these two models, except for a few instances where the values of the lithofacies group bodies can be seen. An example of the difference in the models is a single cell layer of low values, roughly 5%, in the estuarine interval of the conditioned model, where there is a layer of moderate values (40 to 55%), just above the -1026 ft elevation line. Similar characteristics were also observed in the models and fence diagrams from the section 24D study area.

Object-based stochastic modeling was used in building the lithofacies, petrophysical, and conditioned realizations. The lithofacies realizations clearly show the vertical heterogeneity of lithofacies groups in the study areas. The lithofacies group shapes are apparent in the

Model Type	Observations & Information	Resolution	Advantages	Disadvantages
deterministic	continuous (scaled gamma ray) log distribution. Shows truncation of layers at unconformities. Not beneficial to integration with seismic using scaled gamma ray data because it does not incorporate geological interpretation.	resolution is based on size of the model, usually a few to tens of feet.	gradational appearance, values more continuous on a large scale compared to petrophysical and conditioned models, models continuous data, would be a sufficient general representation of basic fluid saturation with different data. Different radiation signature in subtidal more evident.	does not incorporate heterogeneities of lithofacies bodies. Continuity is not realistic. Does not incorporate geologic features, just values represented by logs, Models continuous data only. Continuous distribution is not necessarily accurate.
stochastic lithofacies	shows interconnectivity, size and shape, and lateral and vertical distribution of lithofacies group bodies as defined by input parameters.	resolution is more detailed than seismic data, but still on the order of 5 to tens of feet within the study areas. Tends to be less detailed when lithofacies bodies are larger.	incorporates geological aspects of investigation from cores and logs. Takes into account all scales of heterogeneity. Allows several realizations of geology to be observed. Realizations do not vary greatly. Useful tool for prediction of geology. Acceptable model for integration with seismic data.	model output based solely on input parameters and random insertion. Sharp appearance. Building of models is limited by hardware capabilities (based on size, shape, orientation of bodies, and grid resolution).
stochastic petrophysics	distribution of lithofacies bodies can be seen with assigned continuous well log values assigned to them.	models do not give an acceptable distribution of scaled gamma ray values given the resolution of this 2000+ x 2000+ ft model. A smaller area might be more acceptable for a petrophysical model.	uses geostatistical techniques to incorporate discrete and continuous data into one model. With different petrophysical data (sonic or density), this model could be beneficial to a reservoir characterization.	does not predict geology, but needs accurate lithofacies model for modeling of petrophysical parameters. Values tend to be far (very low) removed from the original continuous log values. Some lithofacies group bodies had scaled gamma ray values that were not correct based on well and core data. Problems in transformation of data.
conditioned	distribution of lithofacies bodies can be seen with assigned continuous well log values. Values in between bodies, where the background lithofacies group occurs, are same as deterministic model.	resolution is similar to that of deterministic models and is based on the model area and grid structure. Greater variability in scaled gamma ray values is better for representing distribution of values.	incorporates both deterministic and stochastic models. Models appear more realistic than strict deterministic models by incorporating the lithofacies group bodies. Shows distribution of petrophysical parameters within lithofacies groups.	values in background lithofacies group average tend to be lower than real scaled gamma ray values. Dependent on accurate lithofacies realization for geological background information. Realizations vary slightly based on lithofacies group realizations.

Table 4: Comparison of the four types of 3D geologic models used in this project.

lithofacies group realizations and are reflected also in the petrophysical models.

The conditioned model of section 36D shows an abrupt, variable character that does not completely reflect the shapes of the lithofacies group bodies. The estuarine interval has several grid blocks that are of a slightly different value than expected, but do not reflect the shape of a body. Some of the same characteristics of bodies occur in both the petrophysical and conditioned models near the base of the estuarine interval where there is a large area of background lithofacies group (burrowed sand, in this case), whose value is reflected in its shape on the lithofacies group model.

4.4 Discussion and Conclusions

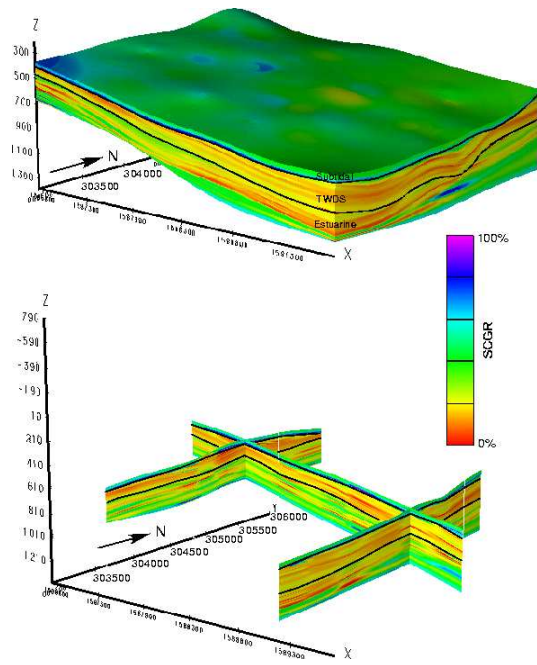
The stochastic lithofacies models and conditioned models are the most suitable types of models of the four methods tested as they will allow integration with seismic data. Deterministic models exhibit a smooth interpolation of the continuous scaled gamma ray values, which may not be an accurate depiction of the subsurface geology because of heterogeneity not sampled by wells. There is not a high degree of lateral continuity in the two study areas, so a strict interpolation technique as used in the deterministic models is not the best method to use.

The stochastic lithofacies models incorporate the heterogeneous characteristics of the subsurface as revealed in core and interpreted from wireline logs by creating multiple realizations with equal probabilistic likelihood. The lateral and vertical heterogeneity of the Temblor Formation is depicted by the distribution of lithofacies group objects in realizations of the stochastic lithofacies which are compatible with cores and wireline logs.

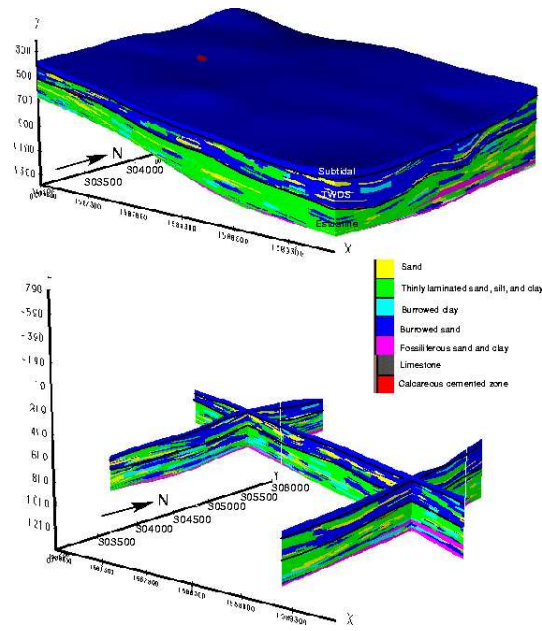
Petrophysical realizations are strongly influenced by distribution of the lithofacies group objects. The calculations of scaled gamma ray values are performed in each of the individual lithofacies group bodies to simulate small-scale variations in scaled gamma ray values. The method allows a representation of scaled gamma ray values in between the wells. The incorporation of geology is a good reason for using petrophysical models with seismic data. However, the values in the final petrophysical models do not always correspond with the expected values of the lithofacies bodies as determined from wireline logs. With the use of petrophysical parameters such as oil saturation, grain size, porosity, and/or permeability, a more useful model could probably be created.

The conditioned models combine the information from both the lithofacies models and the deterministic scaled gamma ray models. The incorporation of discrete geologic parameters and the continuous petrophysical parameters show the distribution of the continuous scaled gamma ray parameter based on geological realizations. The values assigned to the lithofacies

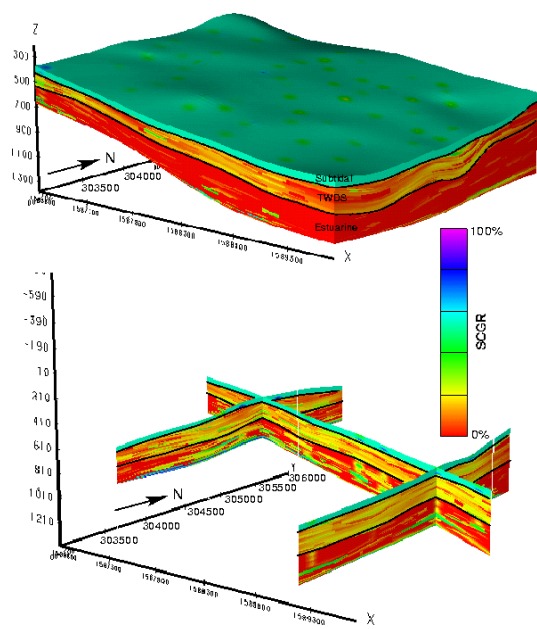
group bodies and the background parameters are consistent with the original continuous log values. This method is useful when modeled with scaled gamma ray logs, but could possibly become even more useful if other logs, such as density, were incorporated.



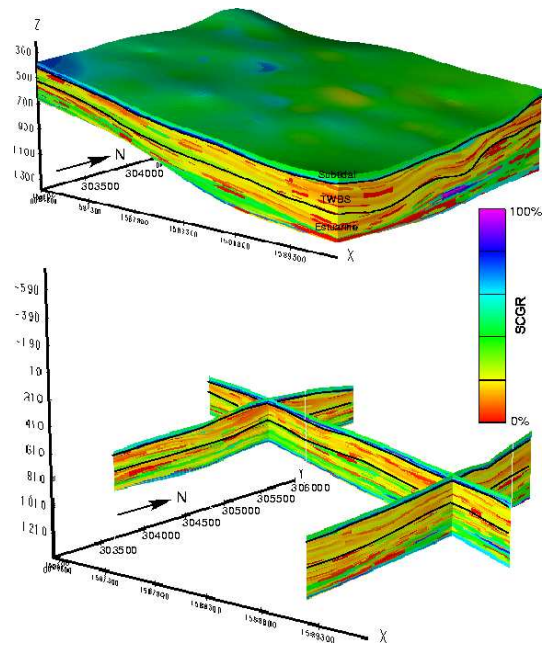
(a) deterministic



(b) stochastic lithofacies

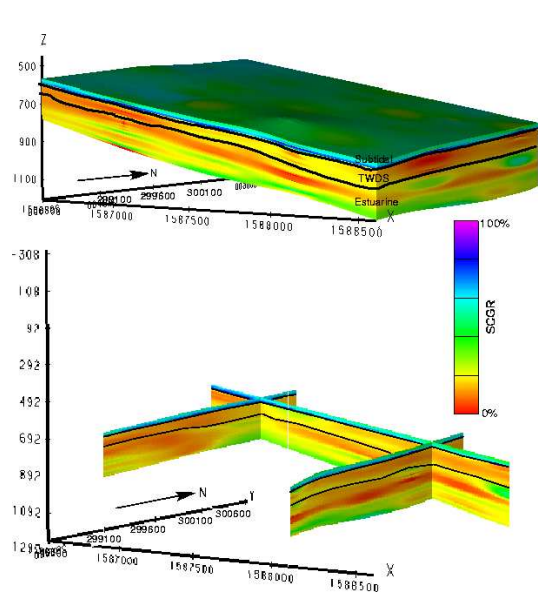


(c) stochastic petrophysics

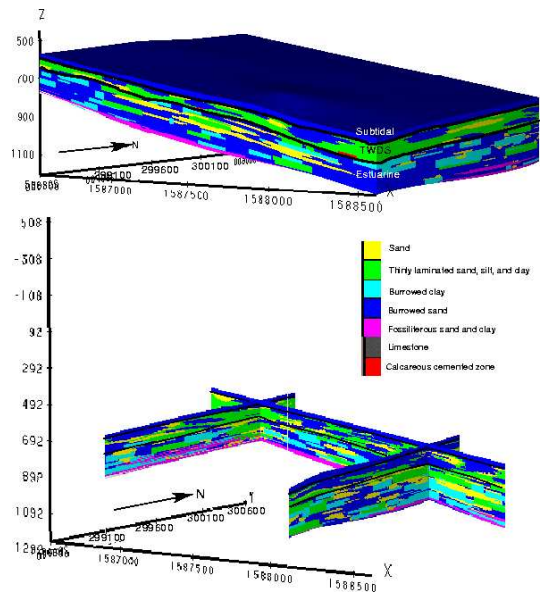


(d) conditioned

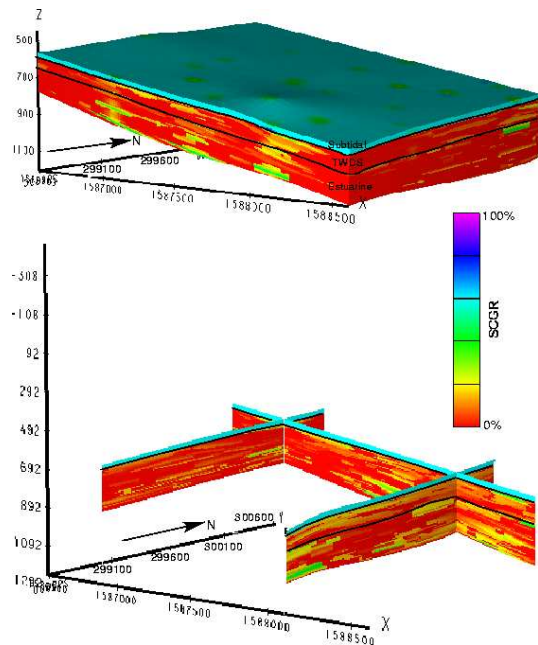
Figure 9: Heterogeneity models for block 25D based only on wireline data. The block size is a quarter square mile.



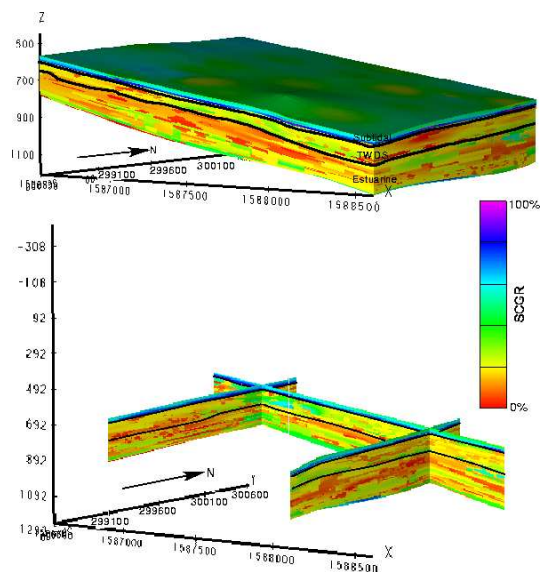
(a) deterministic



(b) stochastic lithofacies



(c) stochastic petrophysics



(d) conditioned

Figure 10: Heterogeneity models for block 36D based only on wireline data. The block size is a quarter square mile.

5 Seismic Heterogeneity

5.1 Introduction

Imhof and Kempner (2003) presented a method to estimate heterogeneity from seismic data. The 3-D seismic volume attributes quantify the heterogeneity contained in the seismic data which could relate to acquisition and processing footprints or stratigraphic and lithologic heterogeneity. If a unit is a composite of small sedimentary bodies, it will contain numerous short-scale variations of the material properties and the seismic heterogeneity attributes may denote average dimensions and orientations of these bodies. The attributes consist of three orientations, three characteristic correlation length scales, and a misfit. They are estimated at every point of interest inside a seismic data volume. Typically, the seismic heterogeneity parameters vary from point to point demonstrating the nonstationary nature of the data, and hence by the assumption, of the reservoir. The heterogeneity volumes cannot only be visualized and interpreted as seismic attributes, but they also allow simulation of stochastic realizations compatible with these nonstationary statistics.

5.2 Attribute Estimation

The heterogeneity attributes are calculated at every point (x, y, z) of a seismic poststack datacube d . A little probe volume v , centered at the current (x, y, z) , is extracted from the full datacube d . This probe v is then crosscorrelated with the datacube d to estimate the local crossvariance function $\hat{\rho}(\Delta x, \Delta y, \Delta z; x, y, z)$ at point (x, y, z) for a number of different correlation lags Δx , Δy , and Δz .

$$\hat{\rho}(\Delta x, \Delta y, \Delta z; x, y, z) = \frac{1}{N(\Delta x, \Delta y, \Delta z)} \times \sum_{\substack{(\delta x, \delta y, \delta z) \\ \in \\ V(x, y, z)}} v(x + \delta x, y + \delta y, z + \delta z) \cdot d(x + \delta x + \Delta x, y + \delta y + \Delta y, z + \delta z + \Delta z) \quad (1)$$

The factor $N(\Delta x, \Delta y, \Delta z)$ normalizes the result with the number of terms used in the summation (1). The averaging or summation volume $V(x, y, z)$ for the current center point (x, y, z) is arbitrary. Large volumes V provide more reliable statistics, but at the price of potentially averaging instationary data. Small volumes reduce the effect of lumping instationary data, but they degrade the resulting statistics due to the smaller amount of data used in the estimation. As a compromise, we often use $V(x, y, z) = v(x, y, z)$, i.e., the summation volume V equals the probe v . The local crossvariance $\hat{\rho}$ is normalized to unity for $\Delta x = \Delta y = \Delta z = 0$ which yields the local crosscorrelation function (*LCCF*) $\hat{R}(\Delta x, \Delta y, \Delta z; x, y, z)$:

$$\hat{R}(\Delta x, \Delta y, \Delta z; x, y, z) = \frac{\hat{\rho}(\Delta x, \Delta y, \Delta z; x, y, z)}{\hat{\rho}(0, 0, 0; x, y, z)} \quad (2)$$

The *LCCF* $\hat{R}(\Delta x, \Delta y, \Delta z; x, y, z)$, however, contains too many values to be of direct use, even if it is computed for only a few lags. To be useful as seismic attributes, the number of values is reduced by fitting the estimate \hat{R} in the least-squares sense with a model *LCCF* \bar{R} which contains only six free parameters. This reduction makes the *LCCF* more manageable and increases the signal-to-noise ratio of the attributes.

Presently, the model *LCCF* \bar{R} is an oriented, anisotropic Gaussian function which allows rapid calculation of *LCCF* models and equiprobable realizations.

$$\bar{R}(\Delta x, \Delta y, \Delta z; a, b, c, \phi_x, \phi_y, \phi_z) = \exp\left(-u^2/a^2 - v^2/b^2 - w^2/c^2\right). \quad (3)$$

The direction are scaled independently with the correlation lengths $a > b > c$ which define the angles ϕ_x (tilt), ϕ_y (dip), and ϕ_z (orientation or northing). The parameters (u, v, w) are obtained from the lags $(\Delta x, \Delta y, \Delta z)$ by rotation with the rotation matrix $\mathbf{S}(\phi_z, \phi_y, \phi_x)$ (e.g.,

Schwarz, 1989).

$$\begin{pmatrix} u \\ v \\ w \end{pmatrix} = \mathbf{S}(\phi_z, \phi_y, \phi_x) \cdot \begin{pmatrix} \Delta x \\ \Delta y \\ \Delta z \end{pmatrix} \quad (4)$$

$$\mathbf{S} = \begin{pmatrix} \cos \phi_y \cos \phi_z & -\cos \phi_y \sin \phi_z & -\sin \phi_y \\ -\sin \phi_x \sin \phi_y \cos \phi_z + \cos \phi_x \sin \phi_z & \sin \phi_x \sin \phi_y \sin \phi_z + \cos \phi_x \cos \phi_z & -\sin \phi_x \cos \phi_z \\ \cos \phi_x \sin \phi_y \cos \phi_z + \sin \phi_x \sin \phi_z & -\cos \phi_x \sin \phi_y \sin \phi_z + \sin \phi_x \cos \phi_z & \cos \phi_x \cos \phi_y \end{pmatrix} \quad (5)$$

The orientation ϕ_z is defined by the direction of the longest correlation length a , i.e., the direction of maximal continuity. The dip angle ϕ_y specifies the dip of the direction of maximal continuity. Finally, the tilt ϕ_x indicates how much the *LCCF* has been rotated around the direction of maximal continuity. By repeating averaging and optimization at every point (x, y, z) of the dataset, one obtains the heterogeneity cubes for the characteristic lengths a , b , and c , the orientation angles ϕ_x , ϕ_y , and ϕ_z , and the minimization error ϵ^2 .

Simulation

Random realizations with a prescribed autocorrelation function (*ACF*) are often computed by convolution of the zero-phase realization with a white-noise volume (Frankel and Clayton, 1986; Kerner, 1992; Ikelle et al., 1993). The autocorrelations described by the heterogeneity cubes, however, vary spatially. To compute realizations based on the heterogeneity cubes, the convolutional approach is generalized:

$$r(\mathbf{x}) = r_0\left(a(\mathbf{x}), b(\mathbf{x}), c(\mathbf{x}), \phi_x(\mathbf{x}), \phi_y(\mathbf{x}), \phi_z(\mathbf{x}); \mathbf{x}'\right) * n(\mathbf{x}') \quad (6)$$

For our Gaussian model *LCCF* (3), the analytical zero-phase realization is:

$$r_0(x, y, z; a, b, c, \phi_x, \phi_y, \phi_z) = \sqrt{\frac{8}{a b c \pi^3}} e^{-2(u^2/a^2 + v^2/b^2 + w^2/c^2)}, \quad (7)$$

where the parameters u , v , and w are obtained by rotation (5) of x , y , and z .

Application to Coalinga Field

Figure 11 presents a subset of the seismic datacube for a focus area with 221 inlines and 71 crosslines. Each CDP box is 60×60 ft (20×20 m) with a temporal sampling interval of 4 ms. The top Temblor horizon at 400 ms has been used to flatten the dataset. The Temblor formations consist of the strong amplitude events below 400 ms with a thickness of up to 200 ms. In this study, we will concentrate on a timeslice at 440 ms, or 40 ms below the top Temblor horizon. At this depth, we expect the upward-coarsening sand bars of the middle Temblor with north-south orientation deposited in a subtidal environment. Figure 12 presents seismic amplitude, instantaneous amplitude, instantaneous frequency, and similarity. Bright instantaneous amplitudes correlate with high similarities and reduced instantaneous frequencies. The effect could be caused by steam which often increases amplitudes by increasing impedance contrasts (Tague et al., 1999). Steam can also reduce instantaneous frequencies by attenuation (Hedlin et al., 2001). Lower frequencies may increase similarity because shifts in phase or time have a lesser effect on the wavelet. The figures also show a distinct difference between the northern (upper) and southern (lower) halves of the area. The northern part exhibits higher instantaneous frequencies, lower instantaneous amplitudes, and lower similarities than the southern part.

Figure 13 presents slices through the heterogeneity cubes at 440 ms for a probe volume of $9 \times 9 \times 9$ samples. For the long correlation length a , we find that the northern half is basically bimodal with correlation lengths around 5 and 40 cdp, while the southern half contains a broad variety of correlation lengths which systematic fluctuations. The intermediate correlation length b basically mimics the long-range estimates a , but with shorter correlation lengths. Heterogeneity is mostly oriented in the north-south direction with minor dips and tilts. Large tilts often appear to be edge effects caused by an incomplete distribution of correlation lags. Since the seismic dataset has only been time migrated, dip and tilt are

pseudo angles and would need to be mapped to real angles. The short correlation length c is not shown because it is fairly constant around $1.5\Delta t$. Data processing, especially deconvolution, tends to reduce the vertical or temporal autocorrelation function toward a spike. All heterogeneity attributes are only presented as time or horizon slices, although they are true volume attributes. But their rapid variation in the vertical direction makes recognition of patterns very difficult. In addition, interpretation of orientation, dip, and tilt from cross sections is typically more difficult than from map views (Imhof and Kempner, 2003).

Finally, Figure 14 presents four equiprobable realizations based on the estimated heterogeneity cubes a , b , c , ϕ_x , ϕ_y , and ϕ_z . To ease comparison with the heterogeneity cubes presented in Figure 13, the realizations are shown as slices at 440 ms depth, or 40 ms below Top Temblor. Each realization is an instationary random field with zero mean and unit variance which yields stochastic volumes with values roughly between -3 and 3 which could be interpreted as some kind of normalized impedance. All realizations were simulated using algorithm (6). Their only differences are the initial white-noise volumes passed through the instationary filter. Comparison of the realizations 14 and the heterogeneity cubes 13 shows that the simulated heterogeneity follows the orientations prescribed by the heterogeneity orientation ϕ_z . Similarly, long correlation lengths coincide with smoother realizations. As one may expect, the realizations in the northern and southern halves of the study area are rather different. In the northern half, we find long-scale heterogeneity with predominant north-south orientation. In the southern half, we obtain mixtures of long and short-scale heterogeneity with more directional variability which allows nonlinear connectivity over large areas.

5.3 Discussion

We observed that second-order statistics estimated from seismic data are highly variable. Clearly, the common assumption of stationary statistics is invalid not only for the entire field, but even within smaller patches. Geostatistical modeling needs to allow for nonstationarity

either by use of nonstationary simulation algorithms, or by segmenting the reservoir into smaller subunits which are internally homogeneous in a geostatistical sense.

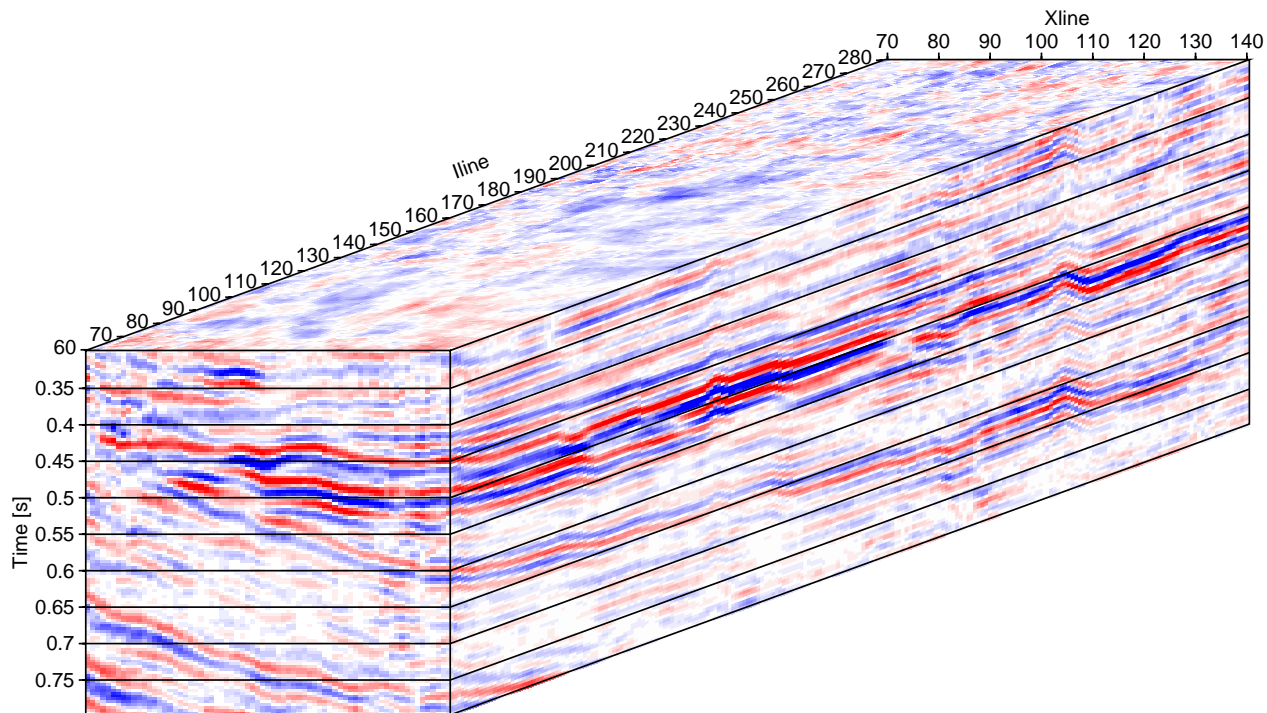


Figure 11: Time-migrated seismic datacube from the Coalinga field. The volume has been flattened at the 400 ms reflector. Red (blue) denotes negative (positive) amplitudes.

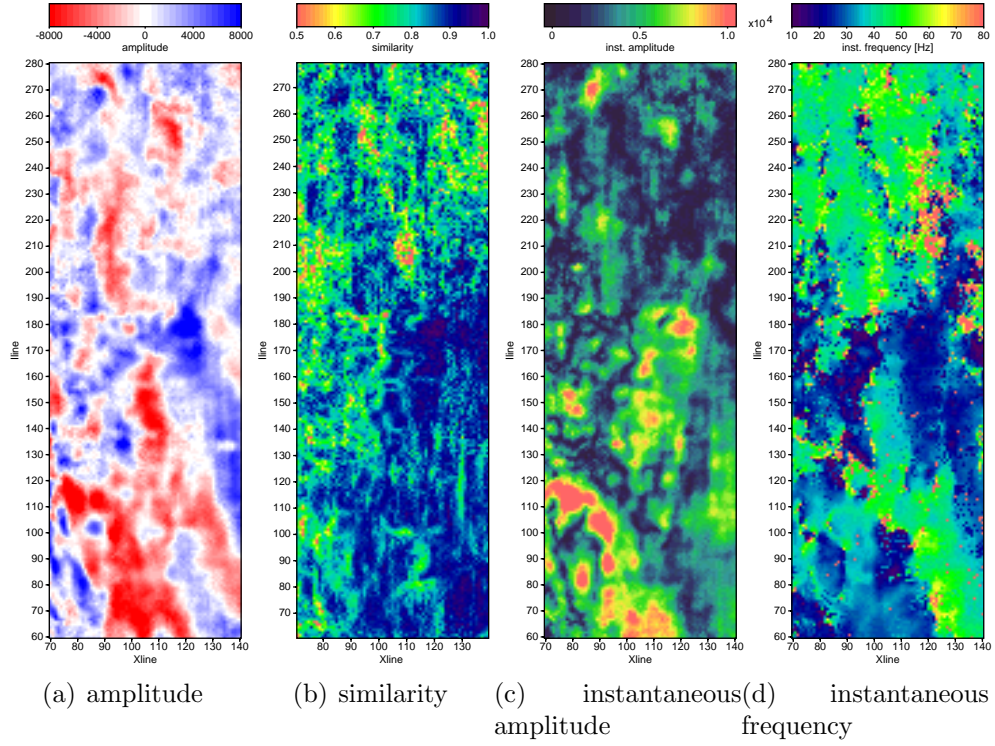


Figure 12: Seismic attribute slices 40 ms below the Top Temblor.

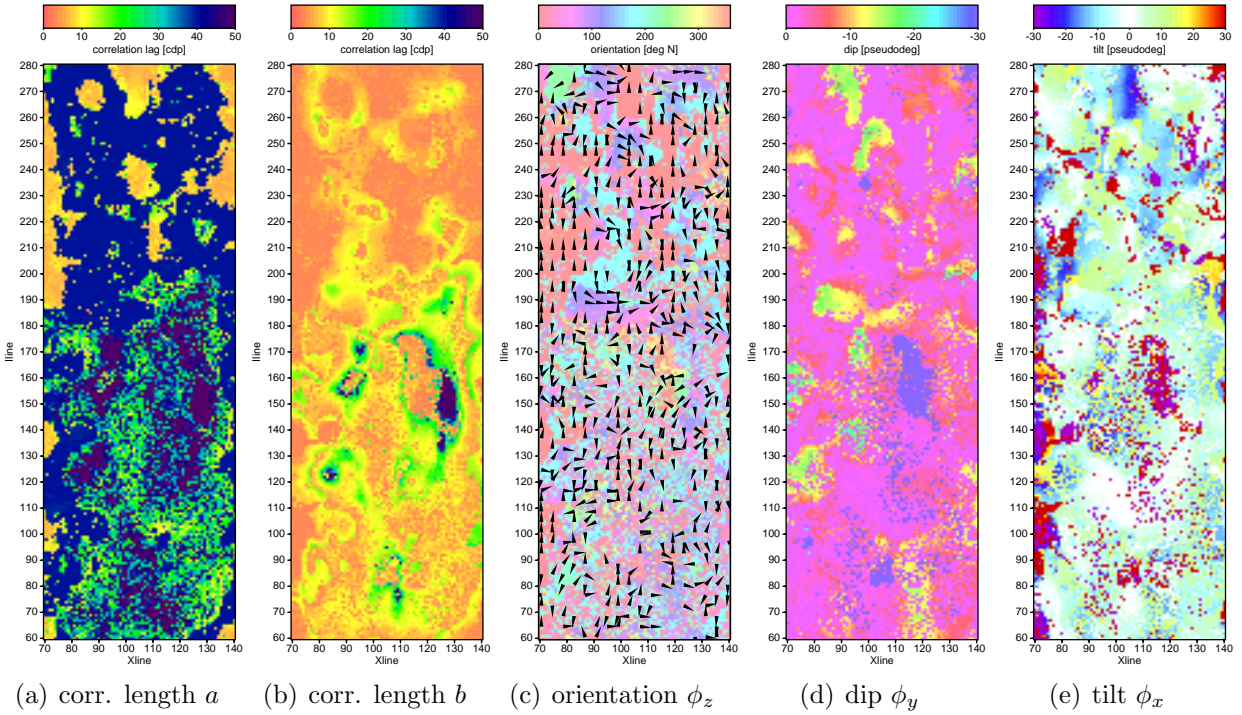


Figure 13: Heterogeneity parameters 40 ms below Top Temblor. Orientation ϕ_z is indicated both by color and arrow direction. A missing arrow denotes vanishing dip.

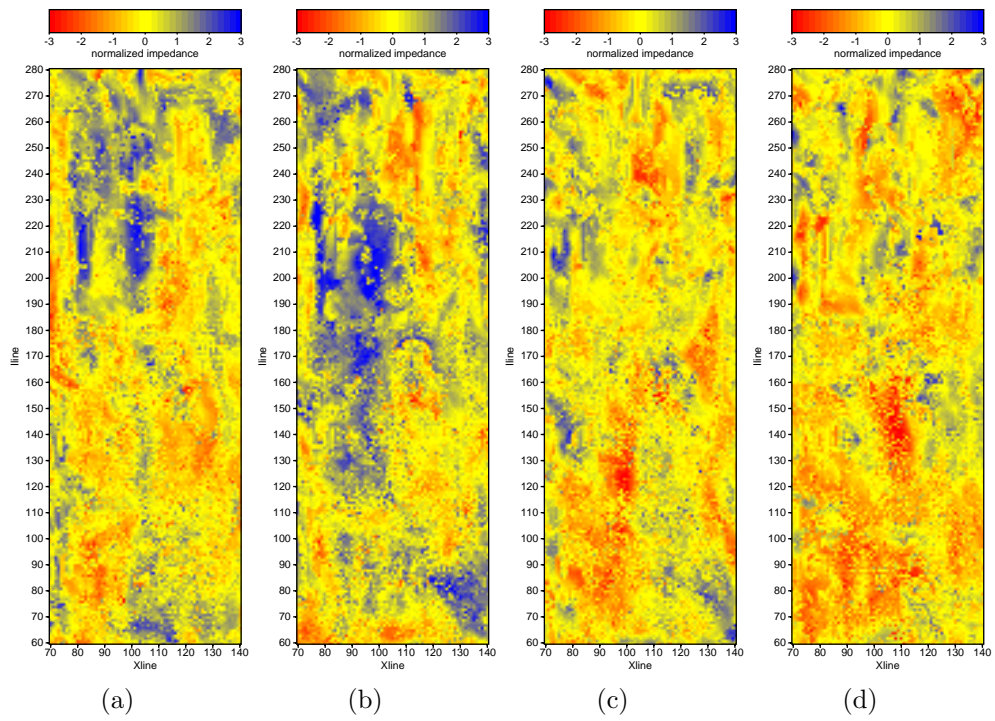


Figure 14: Different realizations which are compatible with the heterogeneity cubes.

6 Seismic Interpretation

6.1 Introduction

The clastic Coalinga reservoir is highly heterogeneous due to deposition of varied lithofacies in different geological time periods when the San Joaquin basin experienced a succession of paleoenvironments ranging from incised fill to subtidal. Localized unconformities segment the reservoir into different petrophysical blocks where reservoir properties differ. Seismic data provide a means of tracing these unconformities between wells and allow 3-D visualization of sedimentary bodies.

The seismic data over Coalinga field was not collected at one time over the entire field. Instead, smaller surveys were acquired over a timespan of five years while the field underwent production and steam injection (Clark et al., 2001). Merging these surveys is challenging (Mahapatra, 2005) as the reservoir has changed between survey phases and the transition zones between surveys give the wrong impression of a severely faulted reservoir. The various amounts of steam injection are also wreaking havoc with seismic amplitudes and frequencies, and hence, with seismic resolution. Moreover, steamed zones slow the seismic waves down compared to virgin ones which would give a perfectly flat layer a very rugged appearance.

Despite these shortcomings, we made extensive use of the seismic data and traced unconformities, mapped sedimentary features, and analyzed seismic attributes to gain a better understanding of Coalinga reservoir, albeit with the awareness that not all details add up. For example, some reflection loops could not be closed without contradicting geological experience. Nevertheless, we gained valuable insights into Coalinga reservoir which heavily guided the other components of this study.

6.2 Seismostratigraphic Interpretation

Starting with the wireline correlation crosssections with examples shown in Figures 5 and 7, we posted the time equivalents of the unconformities onto the merged seismic data for iden-

tification of Base Temblor, Buttonbed, Valv, and Top Temblor. While trying to map these unconformity surfaces on the seismic data, we observed severe misties and reflector discontinuities because the seismic 3-D data set was actually merged from different surveys acquired at different times in a geologically complex area with multiple phases of steam injection. Mapping the unconformities turned out to be problematic. Rather than reprocessing all the data which would not have helped with the reservoir changes, we an interpretation trick. We assumed that the strata underneath the Coalinga reservoir are simple without structural complexity, and flattened these reflections. Many of the apparent faults in the Coalinga reduced their throws or vanished completely which improved linkage of seismic features across transition zones between surveys (Mahapatra et al., 2003).

After application of this flattening technique, the four Temblor unconformities observable on the seismic data were mapped. We confirmed that the reservoir is indeed compartmentalized into three major vertical chronostratigraphic sequences as illustrated on Figure 15. We noticed that in the western part of the seismic coverage area, the Buttonbed and Valv unconformity surfaces appear to be merging which implies that a portion of the Buttonbed unconformity has been eroded by the overlying Valv unconformity (Figure 15).

We observed offlap, onlap, and reflector-truncation relationships against the unconformities suggesting that that are sequence boundaries. Figures 16 and 17 present examples of these relationships. The zone between the Buttonbed and Basal Temblor surfaces, which consists of incised valley fill and estuarine facies (Table 3, contains channel cuts as shown in Figure 17. In the lower central part of the study area, these channels appear to be re-cut and re-stacked. Careful analysis indicates that the depositional direction seems to be changing slightly over the field for different geologic time of deposition from NW-SE to SW-NE.

6.3 Seismogeomorphic Interpretation

Seismic attributes are useful for qualitative interpretation of seismic data. They are derived from basic seismic measurements. They measure different aspects of the seismic trace and

provide a different look at the data. They help to ascertain structure, lithofacies, or reservoir parameters because their responses vary widely with variation in lithology, geometry and structural pattern of deposition, or lithofacies (e.g., Brown, 1999). For the highly heterogeneous clastic Coalinga reservoir, we used instantaneous amplitudes and related attributes to delineate lithologies and steam, instantaneous frequency to map steam, and instantaneous phase to ascertain lateral continuity. We also tried to use seismic coherency data, but found that the discontinuities caused by the data merging made interpretation difficult. Some examples are shown in Figure 12.

3-D attribute visualization proved to be the most effective technique to analyze sedimentary patterns and bodies. For example in Figure 18, we observed multiple channel stack geometry patterns. Looking in a northeastern direction into the reservoir, I found two prominent channel systems, a major one on top and a minor one in the bottom part of the reservoir. The major one seems to be laterally and vertically extensive and gradually shifts towards an ESE-SE direction. The minor one is only seen towards the west part of the seismic coverage area and appears to shift toward SSE.

The instantaneous amplitudes for the whole datacube for the seismic coverage area are shown in Figure 19 which illustrates the generic stratification pattern of the reservoir. Figure 20 shows that rendering low instantaneous amplitudes in a transparent manner reveals distinct distribution patterns for the seismic lithofacies over the field. The most prominent and vertical extensive pattern is at the top. The vertical extension of the bottom one is less compared to the one on top. These bodies rendered in yellow appear to collocate with clastic reservoir sands. The upper seismic facies body overlies the Buttonbed surface and thus coincides with both the wave-to-tide dominated facies tract and the subtidal facies tract. The lower seismic facies body coincides with the incised valley fill deposits. The transparent seismic facies body between 550-700 ms in Figure 20 (sandwiched in between the top and bottom reservoir rocks distribution) appears to represent the estuarine deposits where only insignificant reservoir sands are normally expected in the area. The absence of prominent

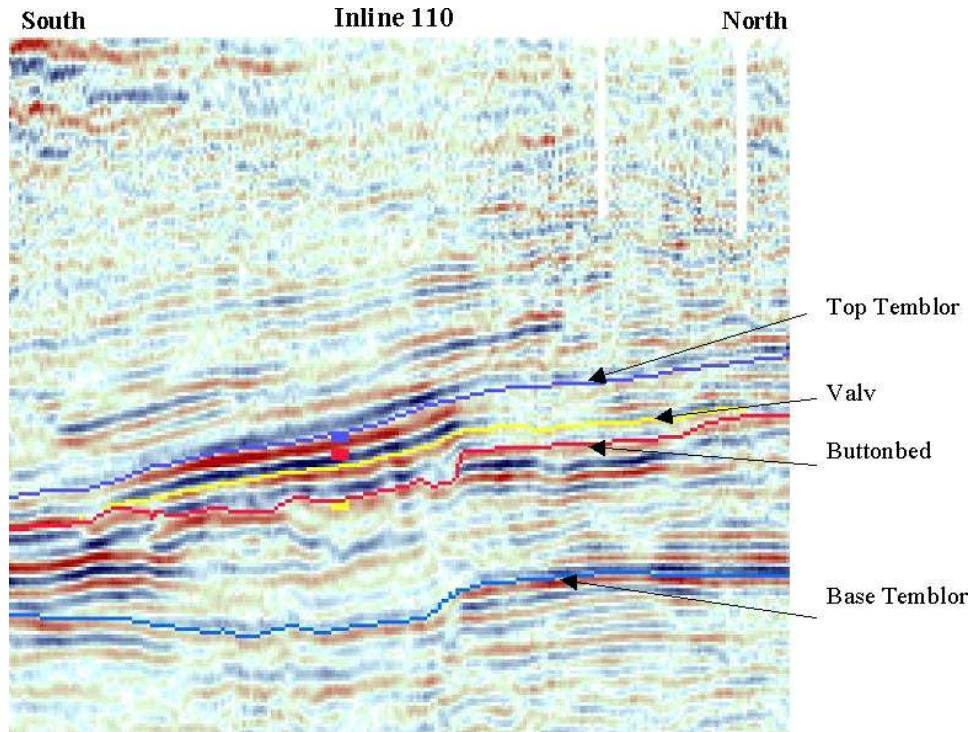


Figure 15: Seismic unconformities within the Temblor formation.

estuarine reservoir rocks in the Temblor of Coalinga field is further evidenced by outcrop, core and wireline log analyses performed by Bridges and Castle (2003). They observed that the estuarine deposit is mainly composed of intercalations of claystone, siltstone, and fine grained sandstone incapable of forming good reservoir rocks.

6.4 Discussion

The seismic data allowed interpolation of the geologic bounding surfaces observed in outcrops, cores, and wireline logs over the entire seismic coverage area by mapping of seismic unconformities. This process was hindered by the merging of chunks of seismic data acquired at different stages of the steam injection program. Lastly, 3-D visualization of seismic instantaneous amplitudes revealed the presence of two seismic facies bodies which appear to represent porous reservoir sands in the lower and upper Temblor.S

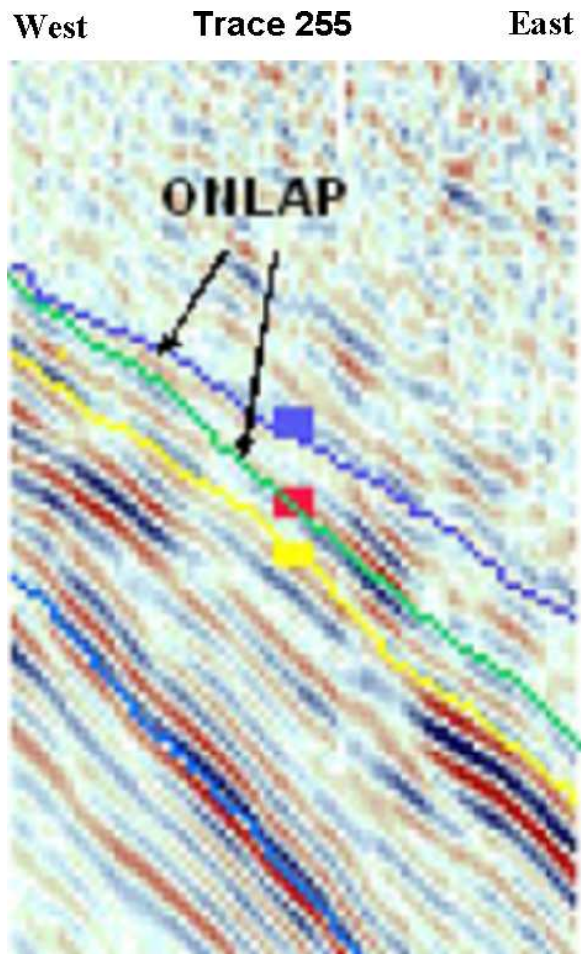


Figure 16: Seismic onlap relationship between Top Temblor (dark blue) and Valv (green). Also shown are the Buttonbed (yellow) and Bottom Temblor (blue) unconformities.

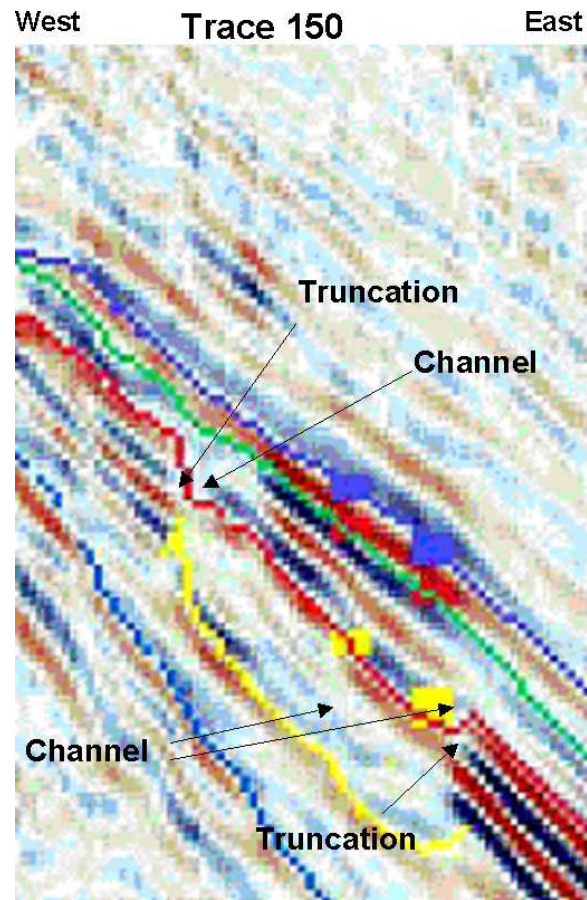


Figure 17: Truncations of channel (yellow) between Base Temblor (blue) and Buttonbed (red). Also shown are the Valv (green) and Top Temblor (blue) unconformities.

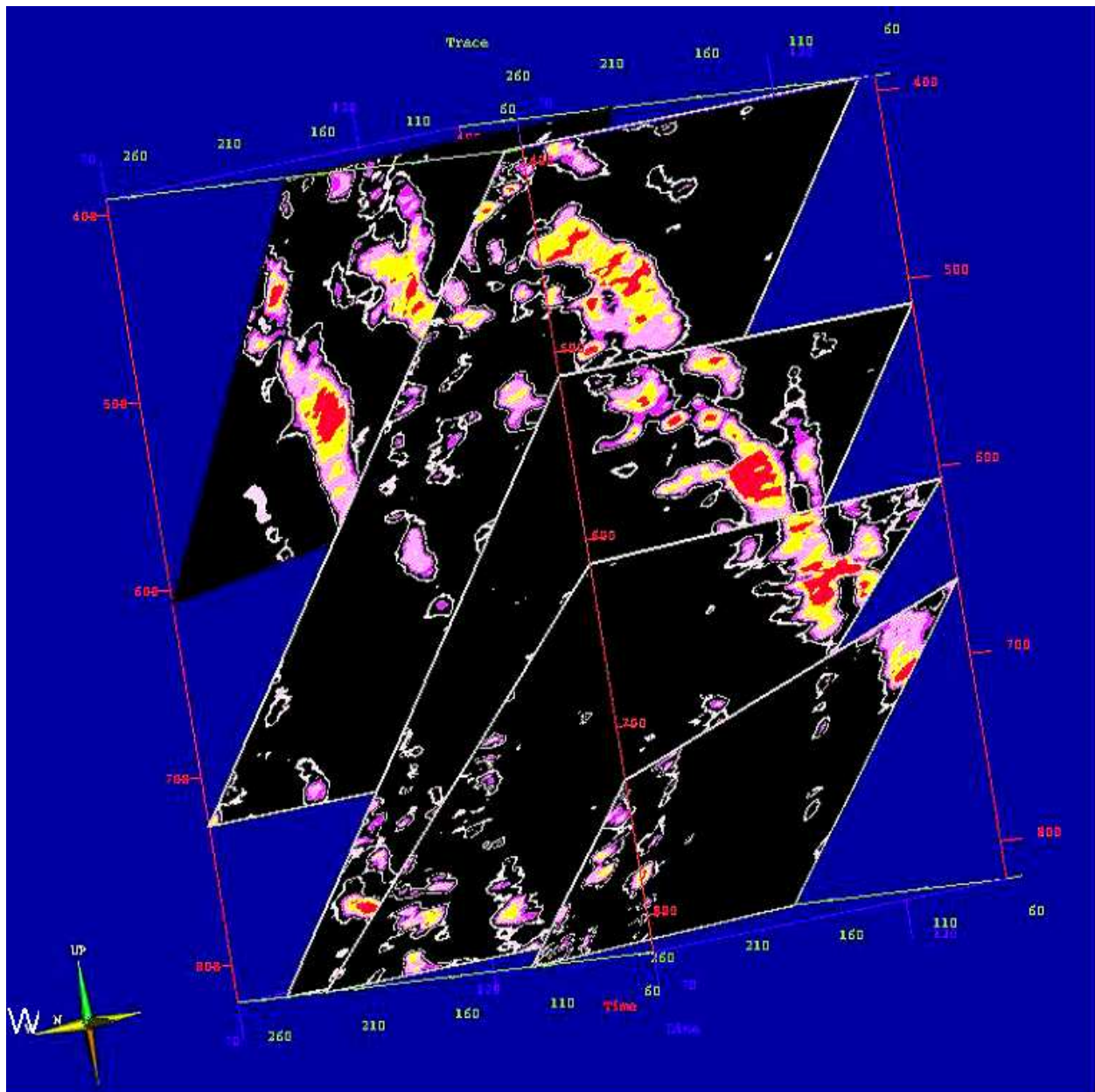


Figure 18: Oblique slices through the seismic instantaneous amplitude data volume. The major channel system is slowly shifting its course towards ESE-SE. A minor channel system is shifting towards SSE.

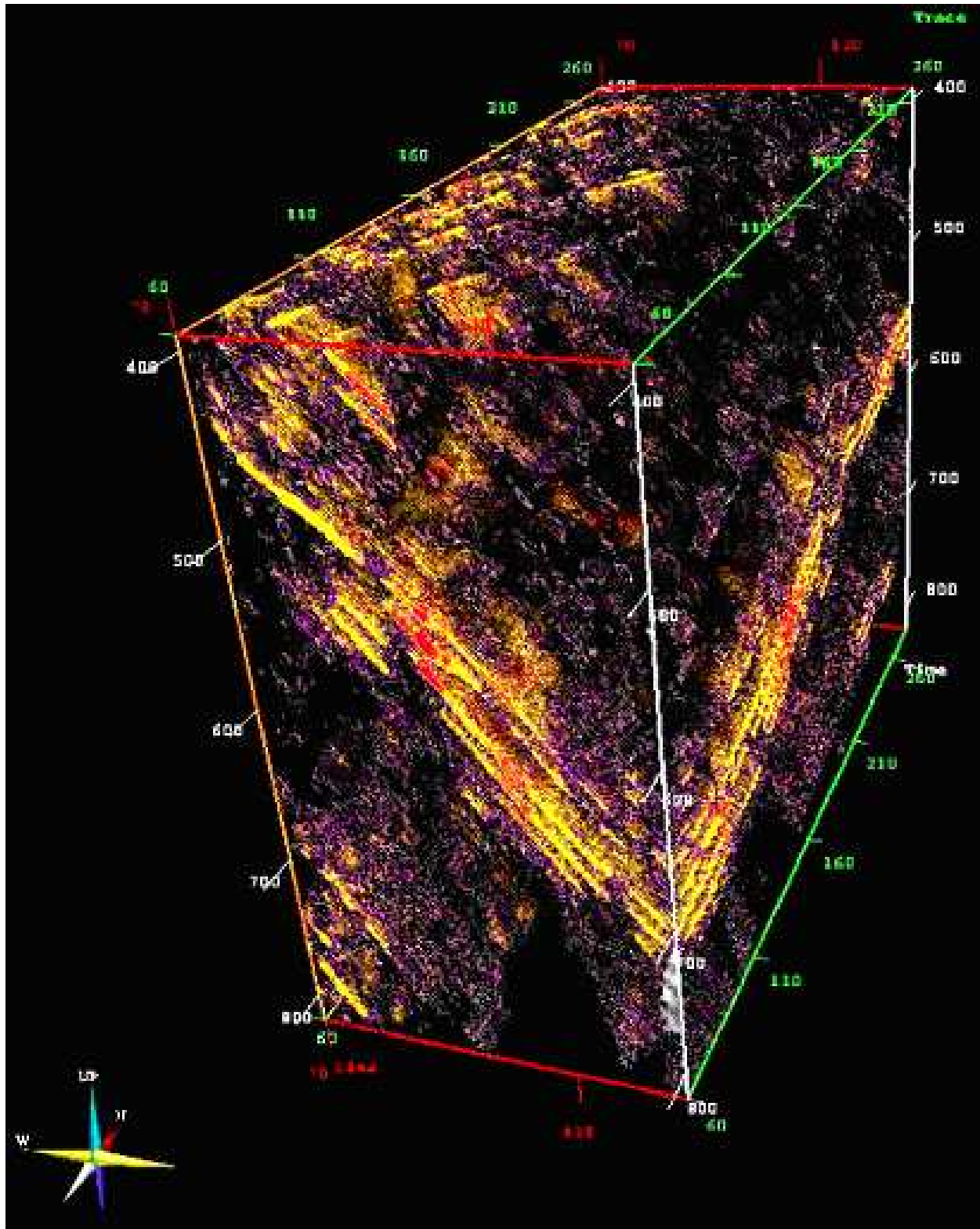


Figure 19: Seismic data volume of the instantaneous amplitude attribute showing the generic stratification pattern underneath the seismic coverage area. The strong amplitudes demarcate the Temblor formation.

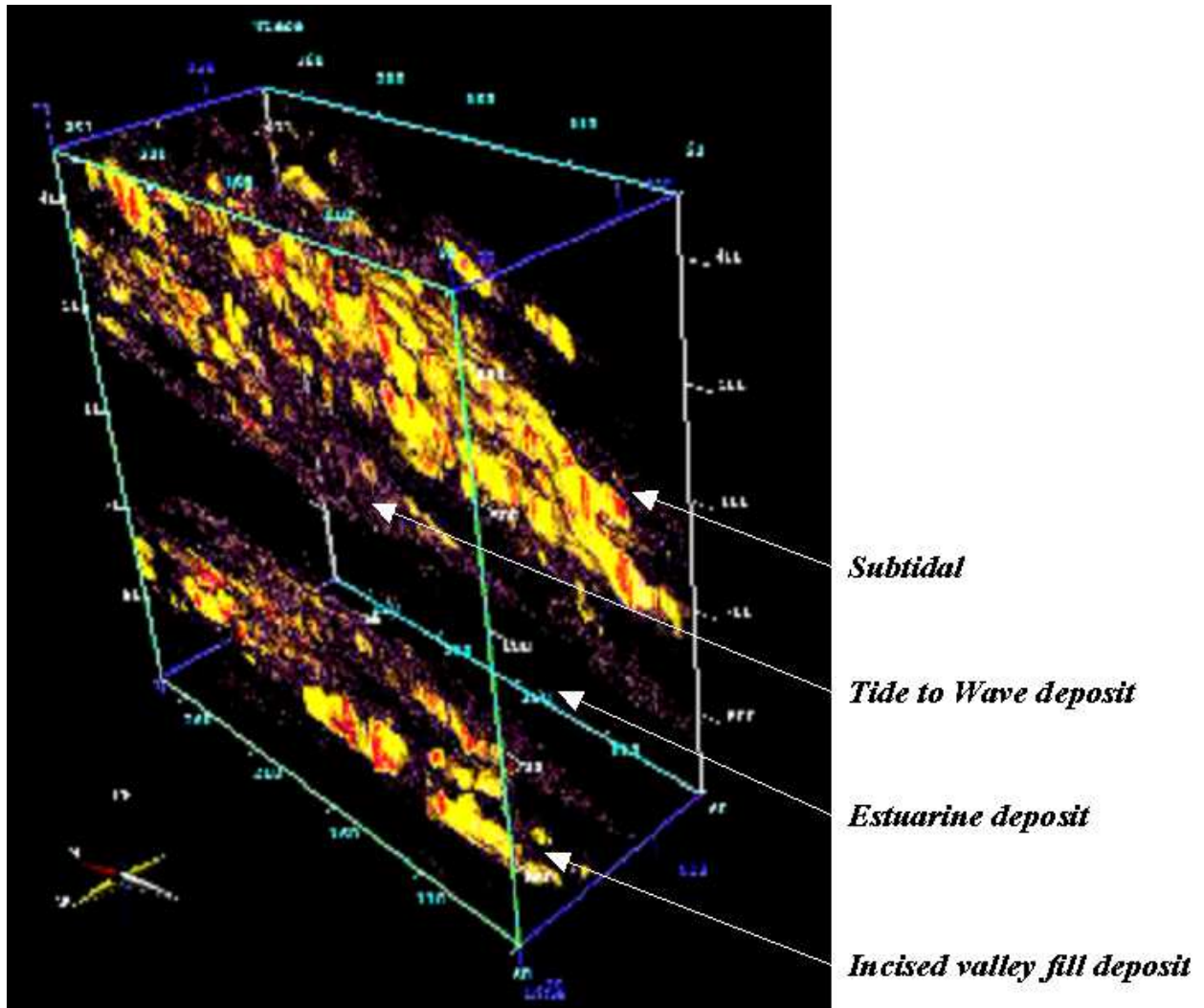


Figure 20: Instantaneous amplitude attribute with low amplitudes rendered transparent. The seismic body on top collocates with the tide-to-wave-dominated and subtidal facies tracts. The lower body collocates with the incised-valley-fill tract.

7 Integration of Geologic Models and Seismic Data

7.1 Introduction

Three data sets were used for integration: (1) lithofacies data from core and outcrop studies, (2) geophysical wireline data, (3) and 3D seismic data . Core and outcrop studies were performed by Bridges (2001) and Mize (2002). Their results were used for definition of the bounding surfaces and lithofacies groups. Wireline data including sonic, density, and gamma ray logs from 71 wells contained in a 1 mile² study area located predominantly in section 36D were utilized first to identify bounding surfaces and lithofacies, and then to create geologic realizations of heterogeneity compatible with wireline and seismic data. Three types of models were created using RMS (2002): deterministic models, stochastic lithofacies realizations, and stochastic composite realizations. Deterministic models distribute information from gamma-ray and density logs throughout the focus volume to provide a representation of lithologic and density variations within the reservoir units. The realizations, however, use geostatistical techniques to incorporate interwell heterogeneity.

7.2 Integrated Heterogeneity Models

Deterministic models are created using continuous well data that results in a single outcome for each realization. Stochastic realizations have the ability to fill in missing data, for example in between wells, not with a single answer but with a suite of equiprobable models that fit the data equally well. Furthermore, the different realizations provide a greater variety of results than the smooth deterministic models and allow multiple scenario analysis. The equiprobable realizations commonly have a realistic texture of heterogeneity in regions that are missing data. Without introducing stochastic heterogeneity, the models become too simplistic displaying facies that are too smooth and continuous or that gently undulate from one well to the next rather than exhibiting the interwell variations.

The simulations introduce heterogeneity through the spatial distribution of the seven

lithofacies groups and their properties. Within the Temblor Formation, the extent and continuity of the sedimentary bodies and the the lithofacies groups have the greatest impact on fluid movement (Mize, 2002). This continuity includes the spatial distributions and the interactions between seven lithofacies groups. Core and outcrop studies as well as well logs provided a means of characterizing vertical features, and stochastic lithofacies models created from these data provided a realization that could be used to identify the distribution of wells at well locations. In areas with minimal well spacing these models even provided some continuity in interwell locations. For larger well spacings, seismic data can be used to locate bounding surfaces and unconformities between wells. The resolution of the seismic data may not provide a direct means of identifying individual lithofacies, but the seismic data can be used as a conditioning parameter when creating stochastic realizations.

We generated many different lithofacies realizations which honored the lithofacies logs at the well locations and displayed realistic continuity of the lithofacies groups compatible with local outcrop data. Realizations conditioned to instantaneous amplitude (e.g., Taner et al., 1979) provided the most geologically reasonable representations of lithofacies continuity because they contain high amounts of spatial variation that is independent of well spacing and well locations. This was demonstrated through the creation of several models with varying amounts of well control. The resulting realizations displayed features in interwell regions based on the instantaneous amplitude data and corresponding facies probability functions, yet in areas where wells were present the well control was honored before the seismic data.

Seismic resolution is measured in terms of seismic wavelength, which is the quotient of velocity and frequency. Seismic velocity increases with depth while frequency decreases with depth. The result is a wavelength that increases with depth making resolution poorer (Brown, 1999). For this reason seismic data cannot resolve small-scale reservoir heterogeneities that exist at depths. However, the statistical properties of the heterogeneities can be inferred statistically from the seismic data. This was done in this study through the creation of facies probability functions, which define the relationship between seismic attribute values

and the probability of encountering a particular facies, at a particular location within the formation. A major component of this study was the development of stochastic composite models that are conditioned to seismic attributes and display stratigraphic interpretations of interwell regions. Mize (2002) created conditioned models using trend modeling where hard data for conditioning was provided only at well locations. By using stochastic composite models that are also conditioned to seismic attributes, the entire distribution of facies is guided ensuring that the probability for simulating lithofacies follows defined facies probability density functions. By creating composite models that use both well and seismic data, a much more reasonable representation of the reservoir is achieved and it is possible to identify and characterize interwell heterogeneities.

7.3 Model Comparisons

We compared several different combinations of data, models, and realizations. They included: (1) a comparison between the raw seismic data and the conditioned models; (2) a comparison between the resulting conditioned models and scaled gamma-ray logs; (3) a comparison of the two study areas by studying the cores and model results to characterize geologic differences; (4) a comparison of the advantages and disadvantages of the three data sets; (5) a comparison of the different types of models created for this project; (6) and comparison between this study and previous work that integrated multiple data sets.

Comparison between Seismic Data and Conditioned Models

We attempted to compare the seismic data cube for the focus area with the resulting conditioned models to check the structure of the bounding surfaces and to evaluate how the models utilized the seismic data. This comparison was complicated because of scale difference between the seismic data cubes and the resulting models (Figure 21). The Temblor formation is very thin in the seismic section, but without vertical exaggeration, details on the realization are obscured and cannot be seen.

Comparison between Conditioned Models and Well Logs

A comparison was also made between the resulting conditioned models and scaled gamma-ray logs. In some areas these comparisons did not prove very useful because the seismic conditioning neglected some of the lithofacies bodies in the wells. An example is a large gamma spike corresponding to the calcareous cemented sand lithofacies. This lithofacies body was not present in the model because no attribute values overlapped with the facies probability density functions for calcareous cemented sand in the subtidal facies of this focus. Use of more data might have prevented this omission.

Comparison of Two Focus Areas

A comparison was made between the two study areas to try to identify the effects steam flooding might have on model results. Core descriptions (Mize, 2002) from wells in each study area were compared in order to identify geologic differences that exist between the study areas that would affect modeling. We found the two areas to differ greatly. For example, in both the subtidal facies tract and the tide- to wave dominated shoreline facies tract, a more complete distribution of calcareous cemented sand is seen in the section 25D area. In addition, the distribution of clay lenses/nodules and burrowed structures differs. Similar differences were also observed in the estuarine facies tract. Most variations between the areas were subtle, however, and below the resolving power of seismic data demonstrating the importance of including as much information as possible to characterize short-scale heterogeneities. We also recognized that that the cores did not characterize large areas. Geologic changes occur over short distances which suggests that the differences in seismic data and heterogeneous realizations are not only the result of differential steam flooding, but also have a geologic component.

7.4 Comparison of Data Sets

Three data sets were used throughout this study including: (1) lithofacies data from core and outcrop studies, (2) wireline log data, (3) and 3-D seismic data, A comparison was made between these data sets to characterize the types of information provided by each, their resolution, and their advantages and disadvantages. While each data set provides important information in characterizing a reservoir, a combination of all three data sets is necessary in characterizing the entire reservoir including small-scale heterogeneities.

Lithofacies data from core and outcrop studies provide the only means of identifying the true geologic features of the reservoir. Cores provide an excellent means of characterizing subsurface lithofacies, but coring every well in the reservoir is not economical and the lateral extent of the lithofacies bodies cannot be determined from cores alone.

Wireline logs are available for every well in the field. However, interpretation of lithofacies displayed on the logs relies on core and outcrop studies. Without them, the general interpretations can be made on the logs (i.e. identifying sand versus shale or limestone), but the small- scale heterogeneities cannot be characterized from well logs alone. In addition, the data collected from logs applies at well locations, and while it may be possible to interpolate facies between wells, short-scale heterogeneity will be overlooked in interwell regions.

3-D seismic data provide continuous and dense amounts of data across the field. However, small-scale heterogeneities cannot be identified with the current resolution of the data. Therefore, interpretation procedures rely on information gathered from well logs, cores, and outcrops to identify bounding surfaces and some of the interwell heterogeneity. For all of these reasons, the only way to characterize small-scale heterogeneities is to combine or integrate all three-data sets as was done in this study.

Model Type	Characteristics & Observations	Advantages	Disadvantages
deterministic	continuous scaled gamma-ray and density distributions	deterministic density models are useful in characterizing seismic response; models created with scaled gamma-ray logs useful in identifying some geologic features	does not incorporate geologic interpretations; does not incorporate lithofacies; wireline interpolation only
stochastic lithofacies	shows some interconnectivity; some lateral and vertical distributions	incorporated geologic information from cores and outcrops; some lateral extent of lithofacies can be identified	works best in small study areas; needs lots of closely spaced wells to characterize heterogeneity
stochastic composite	continuous lithofacies are distributed in interwell regions; models honor both seismic and wireline log data	incorporated geologic information from cores and outcrops as well as seismic data; models are more geologically reasonable because they contain high amounts of spatial variation independent of well spacing and well locations	requires large amount of input data including seismic data; results are dependent on the accuracy of input parameters; rely on accuracy of facies probability density functions

Table 5: Comparison of modeling techniques

7.5 Comparison of Modeling Methods

Three model types were created for this part of the project: (1) deterministic, (2) stochastic lithofacies, and (3) stochastic composites. A comparison was made between these three modeling methods (Table 5). Deterministic models and stochastic lithofacies realizations are controlled only by well data, and therefore, heterogeneity between wells is inferred and the resulting realizations may not reflect true geologic features within the reservoir. Stochastic composite models are conditioned to both well and seismic data, and should provide the most geologically reasonable representations of lithofacies continuity and heterogeneity.

7.6 Discussion

Integration combines different datasets to improve accuracy and reduced uncertainty compared to any single dataset. While geologic models of Coalinga field include a wide range of geologic information collected from well logs, core and outcrop studies, uncertainties persist with regard to interwell heterogeneity. The resolving power of seismic data, however, is inadequate to characterize short-scale reservoir heterogeneity, although some of its statistical properties may be inferred from the seismic data.

The process of integrating geologic and seismic data follows neither a linear nor a hierarchical workflow. Instead, it involves multiple steps and processes including the use of well data in the identification of bounding surfaces on seismic traces, the use of seismic horizons

to define modeling grids, and the creation of stochastic composite models. These lithofacies models are compatible with lithofacies logs obtained from wireline logs. The placement of lithofacies bodies is conditioned on seismic attributes through use of prespecified probability density functions relating lithofacies to attributes. These density functions are either model based or estimated from the data. These realizations are useful in characterizing interwell heterogeneity because they provide stochastic representations of these areas and show the continuation of lithofacies bodies not sampled by wells.

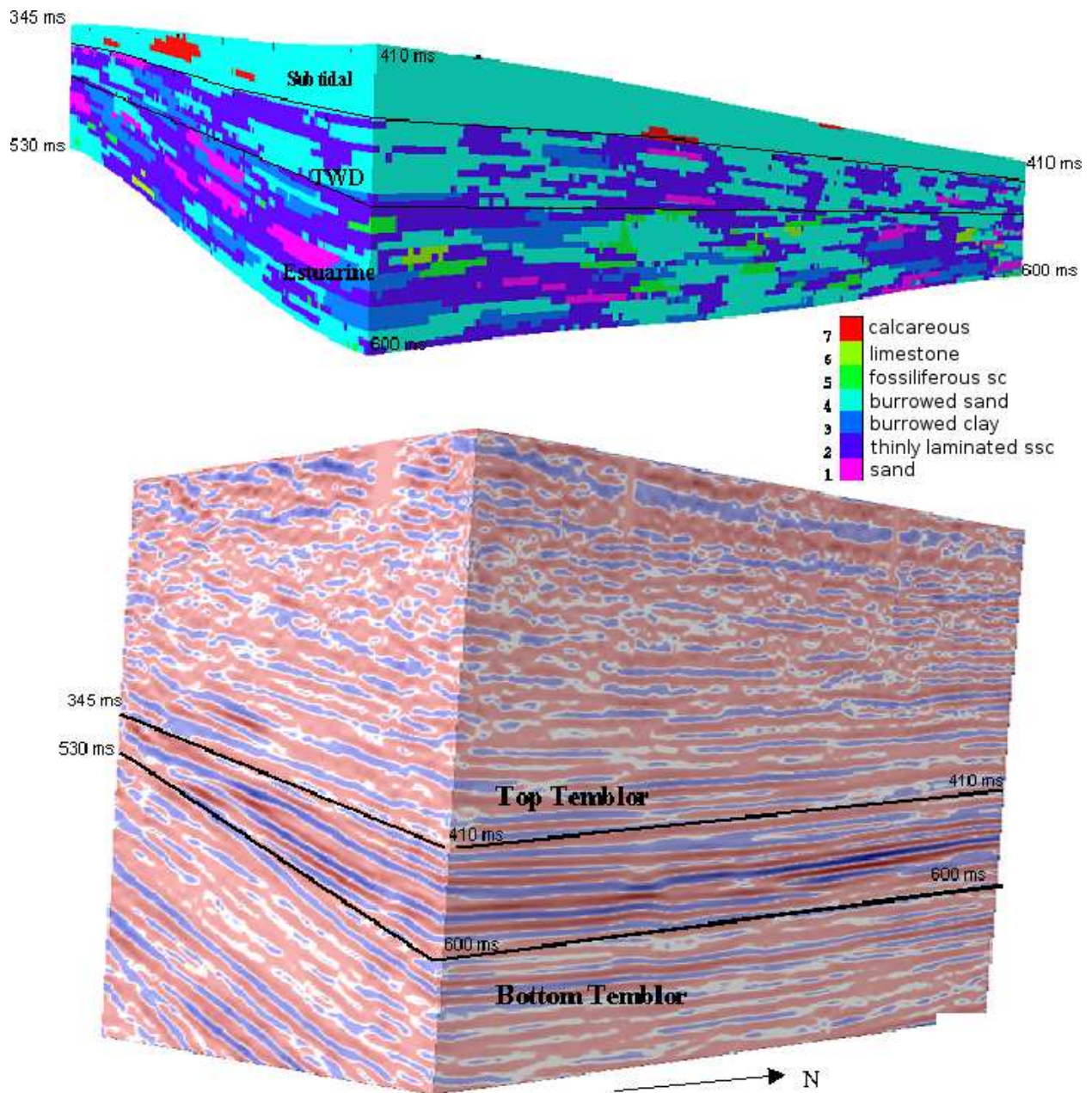


Figure 21: Lithofacies group realization and seismic data from the 1 mile² focus area predominantly in section 25D. The realization is compatible with the wireline-based lithofacies logs and conditioned on the seismic instantaneous-amplitude attribute.

8 Object-Based Stochastic Facies Inversion with Parameter Optimization

8.1 Introduction

Object-based reservoir models build a realization by emplacing geologically meaningful geometric shapes representing channels, barriers, and other geologic objects using geometric and stochastic parameters such as distributions of thickness, sinuosity and/or aspect ratio. The simulations are typically conditioned with wireline and seismic data which boils down to randomly emplacing objects with parameters randomly drawn from prescript probability density functions until all wireline constrains are satisfied and a certain match between realization and seismic data is achieved. This match can be improved by iterative optimization of the parameter probability functions. For Coalinga field, we found that the match can be improved by 20%.

The following sections discuss a pilot implementation and testing of such an optimization scheme (Nowak, 2004). Many questions remain unresolved and will need to be resolved later. For example, which seismic attributes should be used: amplitudes, impedance, or something else? Should seismic attributes be used for both the conditioning of realizations and the improvement of parameters? We believe, however, that the outlined approach to the optimization of geometry parameters and their distributions will generate reservoir models with improved realism and increased correlation between predicted and recorded production histories.

8.2 Process

The algorithm for generating a reservoir realization consists of two loops as depicted in the schematic shown on Figure 22. In the outer loop (shown in blue), we optimize the set of model parameter distributions. In the inner loop (shown in red), we optimize the

realization for a given set of parameters by conditioning with wireline and seismic data. The inner loop generates an object based realization, which for simplicity, is obtained using the industry standard Roxar software (RMS, 2002), although other software should perform equally well. The objects are distributed in accordance to specified volumetric proportions, statistical distributions for the parameters, and placement rules which govern clustering. The resulting realization honors a set of interval facies logs and is constrained by external seismic attributes. The volumetric proportion of the facies are simply estimated by the linear footage of the facies present in the logs. Placement rules are suggested by the facies environment and geologic interpretation. The software module simply adds geometric objects representing geologic bodies into the volume in a random manner. Location, orientation, and geometric size parameters are drawn from the specified distributions. A placed object which is incompatible with the wireline or seismic constraints is simply dropped. The software adds objects until the prespecified volumetric proportions are satisfied.

The algorithm then returns to the outer loop with the optimal realization. Because the inner loop conditions its realizations perfectly to the wells, a portion of all available wells were excluded in the conditioning process for exclusive use in the outer loop. This outer loop optimizes the probability density functions for geometrical parameters, such as aspect ratios and orientations, by nonlinear optimization, for example by simulated annealing (e.g., Otten and Ginneken, 1989).

8.3 Application to the Coalinga Field

Based on the wireline log interpretations of Mize (2002) and Piver (2004), seven lithofacies types occur in the basal zone of the Temblor formation. Because the laminated sands, silts and shales are the dominant facies at 49.7% in this basal zone, they are treated as the background material into which the other facies types are emplaced. They are modeled as rectangular prisms with ranges of aspect ratios and orientations specified in Table 6. Due to the relatively rare occurrence of limestone and calcareous cemented sand (< 2%), their aspect

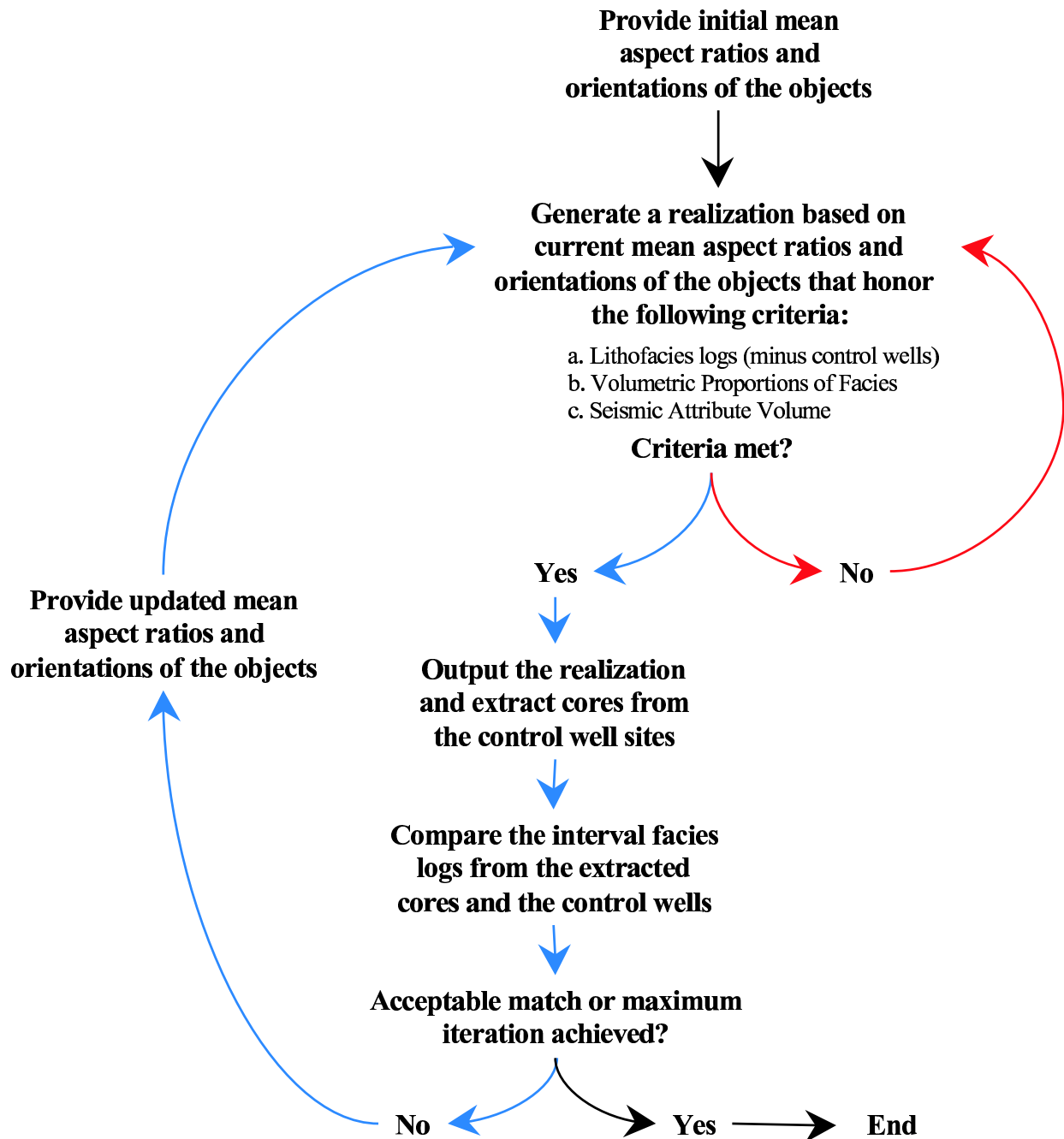


Figure 22: Schematic depicting the object-based stochastic facies inversion and optimization with the inner loop for the realization in red and the outer one for the parameter distributions in blue.

Table 6: Parameters and ranges for the basal zone of the Temblor formation. The dominant laminated sand, silt, and shale group is used as background into which other lithologies are embedded.

Lithofacies Group	Index Number	Volume Fraction (-)	Mean Length (m)	Mean Width (m)	Mean Thickness (ms)	Orientation (°)
Sand	1	0.085	36.5 – 91.4	36.5 – 91.4	3.0 – 8.5	0 – 90
Laminated Sand, Silt and Shale	2	0.497	NA	NA	NA	NA
Burrowed Clay	3	0.147	36.5 – 204.2	36.5 – 204.2	3.0 – 16.8	0 – 90
Burrowed Sand	4	0.196	36.5 – 204.2	36.5 – 204.2	3.0 – 16.8	0 – 90
Fossiliferous Sand and Clay	5	0.058	36.5 – 64.0	36.5 – 64.0	3.0 – 5.8	0 – 90
Limestone	6	0.015	36.5	36.5	3.0	0
Calcareous Cemented Sand	7	0.002	36.5	36.5	3.0	0

ratios are kept constant and small to stabilize the realizations. The standard deviations associated with these aspect ratios and orientations were fixed to 20% their respective mean values.

For this pilot application, we chose a seismo-facies volume for seismic conditioning. This seismo-facies volume was estimated by multiple regression analysis (Emerge, 2000) which allows prediction a core or well attribute such as interval facies from any combination and number of seismic attributes. We selected the following attributes: integrated absolute amplitude, integrate trace, instantaneous response frequency, instantaneous dominant frequency, quadrature trace, perigram², and instantaneous amplitude⁻¹ (e.g. Taner et al., 1979).

Due to time considerations, we performed nine outer loops (\approx 168 hours continuous CPU time) and achieved a 51% match between the nine interval facies logs omitted from the inner loop and the final realization. This result represents a 19% improvement over the initial realization with a mismatch 32%. Remember that this initial realization was optimal

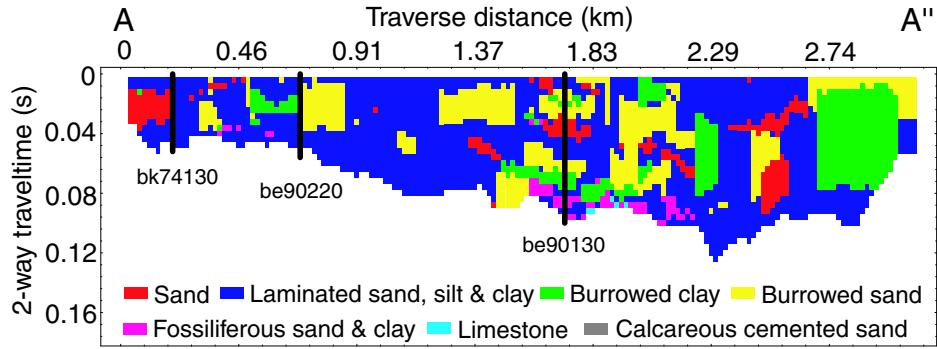
Table 7: Optimized parameters used to generate the final realization for the basal zone of the Temblor formation with has a 51% match to the control logs excluded from the inner loop which represents a 19% improvement to the initial realization.

Lithofacies Group	Index Number	Mean Length (m)	Mean Width (m)	Mean Thickness (ms)	Orientation (°)
Sand	1	36.5	36.5	8.5	30
Laminated Sand, Silt and Shale	2	NA	NA	NA	NA
Burrowed Clay	3	82.3	189.0	12.2	70
Burrowed Sand	4	51.8	189.0	3.0	90
Fossiliferous Sand and Clay	5	51.8	51.8	5.2	70
Limestone	6	36.5	36.5	3.0	0
Calcareous Cemented Sand	7	36.5	36.5	3.0	0

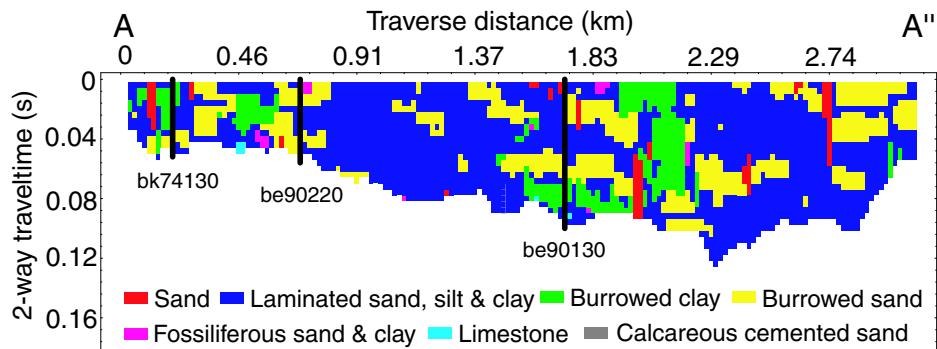
for the initial set of parameters with a perfect fit the the well data used in the inner loop and conditioned to the seismic-facies volume! The statistical parameters used for the final realization are listed in Table 7. Figure 23 depicts a cross-section through the initial and final realization intersecting three of the omitted control wells. The extracted and omitted interval facies logs from these well locations are enlarged and depicted in Figure 24. The matches between the control logs and the realization are marginal at best, however after nine iterations, the realizations become strikingly similar to the control logs which demonstrates the significance of a 19% improved correlation between the facies interpretations at the control points and synthesized data.

8.4 Discussion and Conclusions

We demonstrated that object-based reservoir models should not only be conditioned to wireline and seismic data, but the parameters and their probability distributions should also



(a)



(b)

Figure 23: Crosssections through (a) the initial and (b) the final realizations intersecting three control wells.

be optimized. Even for poor parameters, the conditioning will yield an excellent fit to the data used for conditioning. In between conditioning points, the fit can still be marginal. Parameter optimization based on control or excluded data allows estimation of parameters which yield more realistic extrapolation between conditioning points.

This improvement, however, comes at a high computational expense. There also remain unresolved research questions. The most pressing one is which seismic attributes to use in the inner and outer loops. Others include the choices of convergence criteria and nonlinear optimization algorithms. Despite the obvious potential for improvements, we believe that the outlined approach can eventually generate reservoir models with improved realism, better predictions, and improved matches against control data.

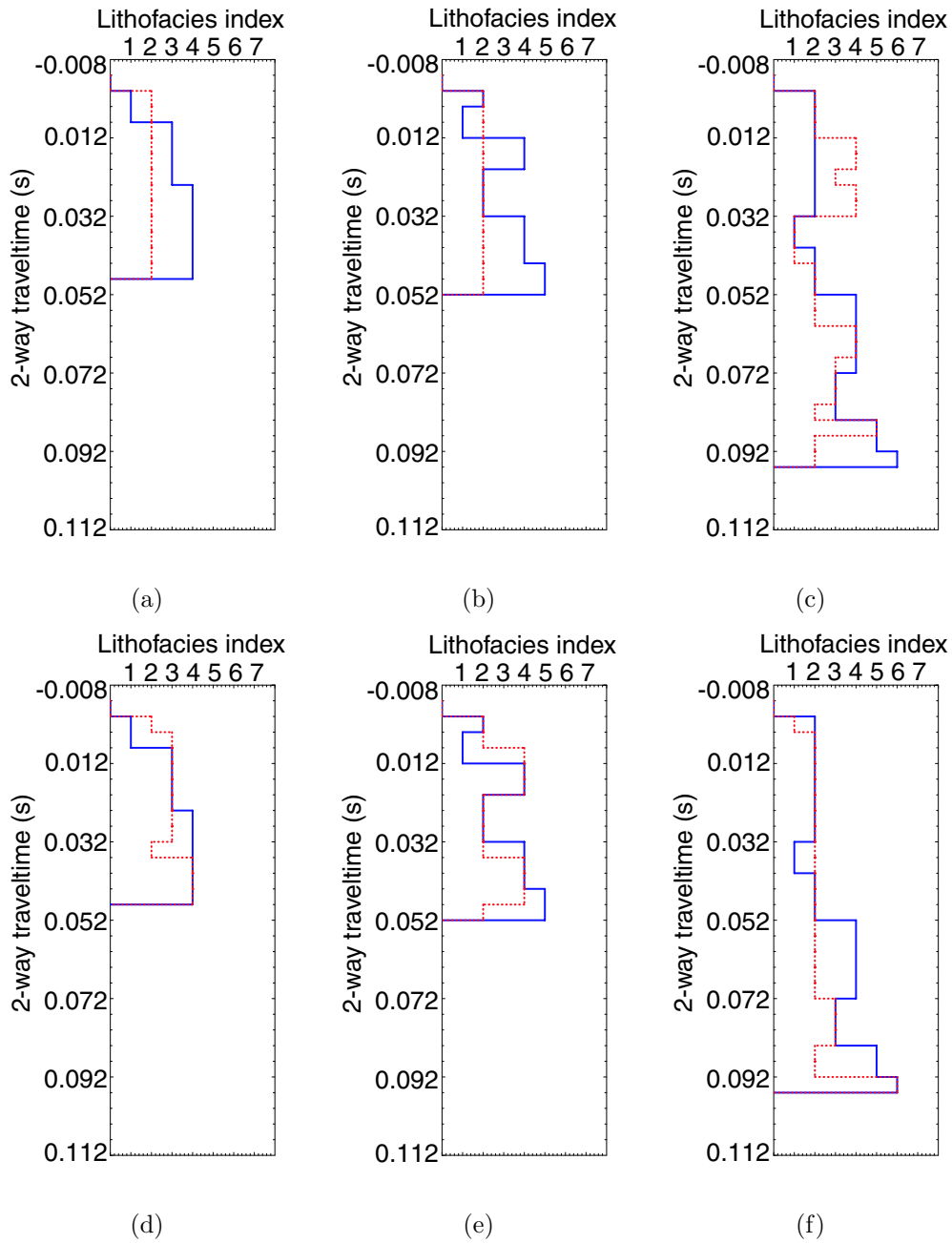


Figure 24: Enlarged view of the control (blue) and simulated (red) interval facies logs from the (a) bk74130, (b) be90220 and (c) be90130 wells for the initial realization and (d) bk74130, (e) be90220 and (f) be90130 well locations for the final realization.

9 Discussion

The original approach to the project was to examine models for the characterization of short-scale reservoir heterogeneity. All these models would have been derived independently. Toward the end of the study, all models would have been compared to determine the best ones. The final stage would have been integration of the winning models. While performing the project, we realized that independent models are impractical. For stochastic simulations based on geostatistical variogram techniques, one needs to know the variogram lags or correlation lengths which could be estimated from seismic data. Variogram-based models can also be conditioned both on wireline and/or seismic data. We found hence, that one kind of model feeds into another one.

Hence, we decided to progress instead in a roughly linear manner through the models. We began with the basic geology of the study area and developed a stratigraphic framework with unconformities and facies tracts. Correlating wireline data, we built a sequence of heterogeneity models, some of which were compatible with individual wireline logs. We used the basic framework to interpret our seismic data which gave us a better three-dimensional understanding of the reservoir geology and the distribution of productive reservoir sands. We also used the seismic data to estimate ranges and orientations for geostatistical variograms. We continued then with geostatistical models, but conditioned both on the wireline data and the seismic data. Finally, we used the seismic and wireline data both to optimize the model parameters as well as to condition the realizations.

The following list of methods for the modeling of heterogeneity is ordered by complexity or computational effort. The order also corresponds to the amount of a priori information needed to perform the simulation. For all these reasons, it would be appropriate to move through this list one model at a time until a realization suitable for the problem at hand is obtained. Each model or realization can serve as a stepping stone for the next one.

Wireline Based Models

Deterministic Models: We used the natural-gamma wireline logs and simply interpolated between the wells. There is only one solution. The procedure is very fast, but model resolution is limited to the distance between wells. The models contain no short-scale heterogeneity.

Stochastic Lithofacies Models: Instead of interpolating or smearing wireline logs between wells, lithofacies bodies are embedded in the realizations. There is an infinite number of equiprobable realizations, all of them compatible with the lithofacies logs at the well locations.

Conditioned Models are based on the stochastic lithofacies models. Within each lithofacies, a petrophysical log such as natural gamma is interpolated between wells by a moving averaging procedure.

Stochastic Petrophysics Models are also based on the stochastic lithofacies models. For each lithofacies, a separate probability density function is used to populate the lithofacies with a petrophysical quantity such as natural gamma. The realizations are both conditioned on the lithofacies logs and on petrophysical wireline log.

Models Based on Seismic Data Only

Heterogeneity Cubes estimate variogram ranges and orientations from seismic data. The estimates can directly be used to generate realizations. The estimates and realizations, however, do not honor unconformities or boundaries between facies tracts and cannot be conditioned to wireline data.

Seismic Interpretation and Visualization allow mapping of unconformities and seismofacies bodies within the resolution of seismic data, which is 10 m or more for the seismic data used. With the help of the geologic framework and wireline data, the seismofacies bodies may be interpretable as, for example, reservoir sands

in certain facies tracts.

Integrated Wireline and Seismic Models

Stochastic Lithofacies Models are similar to the strictly wireline-based stochastic lithofacies models, but the placement of lithofacies bodies is guided by the seismic data through the use of a probability density function which relates one seismic attribute to lithology. Simulations can take a long time, however, as most geologic objects placed in the model will ultimately be rejected.

Optimized Stochastic Lithofacies Models do not only try to find realizations compatible with seismic and wireline data, but also attempt to tweak the stochastic modeling parameters to obtain a better match. Nearly any set of modeling parameters can yield realization which are compatible with wireline and seismic data, but these realizations can be geologically unrealistic. The optimized models will have the highest degree of realism, but their computation is extremely time consuming because many Integrated Wireline and Seismic Models need to be simulated for many different combinations of input parameters.

Our study did not address one crucial step: independent validation of our findings. Independent proof could be obtained by fluid flow simulations, followed by matching the production or steam injection history. Finding bypassed or new reserves would be another kind of validation. The first main finding of our project, however, is not so much which method of heterogeneity characterization is better than the others, but rather that we really needed an excellent understanding of the geologic framework which was constantly refined by findings from the modeling studies. Second, results from each modeling step were later used again to determine or constrain input parameters for more advanced simulations.

10 Bibliography

E. H. Bailey, W. P. Irwin, and D. L. Jones. Franciscan and related rocks, and their significance in the geology of western California. California. California Division of Mines and Geology Bulletin 183, 1964.

J. A. Bartow. The Cenozoic evolution of the San Joaquin Valley, California. U.S. Geological Professional Paper 1501, 1991.

M. A. Bate. Description of field trip stops 1, 2, and 3. In *SEPM Field Trip Guidebook No. 3, 1984 Midyear Meeting, San Jose, California*. SEPM, Tulsa, OK, 1984.

M. A. Bate. Depositional sequence of Temblor and Big Blue formations, Coalinga anticline, California. In S. A. Graham, editor, *Geology of the Temblor Formation, Western San Joaquin Basin, California*, volume 44, pages 69–86. Pacific Section SEPM, Tulsa, OK, 1985.

R. G. Bloch. *Studies of the stratigraphy and structure of the San Joaquin basin, California*. PhD thesis, Stanford University, 1999.

R. A. Bridges. Sedimentology and reservoir characterization of the Miocene Temblor Formation, Coalinga, California. Master's thesis, Clemson University, 2001.

R. A. Bridges and J. W. Castle. Local and regional tectonic control on sedimentology and stratigraphy in a strike-slip basin: Miocene Temblor formation of the Coalinga area, California, U.S.A. *Sed. Geol.*, 158(3-4):271–297, 2003.

A. R. Brown. *Interpretation of Three-Dimensional Seismic Data*. Society of Exploration Geophysicists, Tulsa, OK, 5th edition, 1999.

J. W. Cady. Magnetic and gravity anomalies in the Great Valley and western Sierra Nevada metamorphic belt, California. Geological Society of America Special Paper 168, 1975.

- M. S. Clark, L. F. Klonsky, and K. E. Tucker. Geologic study and multiple 3-D surveys give clues to complex reservoir architecture of giant Coalinga oil field, San Joaquin Valley, California. *The Leading Edge*, 20(7):744–751, 2001.
- T. A. Cross and R. H. Pilger. Constraints on absolute motion and plate interaction. *Am. J. Sci.*, 278:865–902, 1978.
- C. L. Current. Characterization of geologic controls on permeability and their incorporation into a three dimensional geologic model of the Temblor Formation, Coalinga, California. Master’s thesis, Clemson University, 2001.
- Emerge. Hampson Russell, Houston, TX, 2000.
- A. Frankel and R. Clayton. Finite difference simulations of seismic scattering: implications for the propagation of short-period seismic waves in the crust and models of crustal heterogeneity. *J. Geophys. Res.*, B 91(6):6465–6488, May 1986.
- S. A. Graham, editor. *Geology of the Temblor Formation, western San Joaquin Basin, California*, volume 44. Society of Economic Paleontologists and Mineralogists, Pacific Section, 1985.
- T. P. Harding. Tectonic significance and hydrocarbon trapping consequences of sequential folding synchronous with San Andreas faulting, San Joaquin Valley, California. *AAPG Bull.*, 60:356–378, 1976.
- K. Hedlin, L. Mewhort, and G. Margrave. Delineation of steam flood using seismic attenuation. In *71st Ann. Internat. Mtg., Soc. Expl. Geophys., Expanded Abstracts*, pages 1572–1575, 2001.
- R. D. Hoffman. Geology of the northern San Joaquin. In *San Joaquin Geological Society Selected Papers*, volume 2, pages 30–45. 1964.

- H. W. Hoots, T. L. Bear, T. L. Bear, and W. D. Kleinpell. Geological summary of the San Joaquin Valley, California. California Division of Mines and Geology Bulletin 170, 1954.
- L. T. Ikelle, S. K. Yung, and F. Daube. 2-D random media with ellipsoidal autocorrelation functions. *Geophysics*, 58(9):1359–1372, 1993.
- M. G. Imhof and W. C. Kempner. Seismic heterogeneity cubes and corresponding equiprobable simulations. *J. Seis. Expl.*, 12(1):1–16, 2003.
- E. H. Isaaks and R. M. Srivastava. *An Introduction to Applied Geostatistics*. Oxford University Press, New York, 1989.
- C. Kerner. Anisotropy in sedimentary rocks modeled as random media. *Geophysics*, 57(4):564–576, 1992.
- P. W. Lipman, J. Prostka, H., , and R. L. Christiansen. Cenozoic volcanism and plate-tectonic evolution of the western United States i. early and middle Cenozoic. *Philos. Trans. R. Soc. of London*, 271A:217–248, 1972.
- S. N. Mahapatra. *Seismic Characterization of Coalinga Oil Field*. PhD thesis, Virginia Tech, 2005.
- S. N. Mahapatra, M. G. Imhof, and W. Kempner. Poststack interpretive static correction. In *73rd Ann. Internat. Mtg., Soc. Expl. Geophys., Expanded Abstracts*, 2003.
- D. E. Marchand and A. Allwardt. Late Cenozoic stratigraphic units, northeastern San Joaquin Valley, California. U.S. Geological Survey Bulletin 1470, 1981.
- M. McWilliams and Y. Li. Oroclinal bending of the southern Sierra Nevada batholith. *Science*, 230:172–175, 1985.

- K. L. Mize. Development of three-dimensional geological modeling methods using cores and geophysical logs, West Coalinga field, California. Master's thesis, Clemson University, 2002.
- E. J. Nowak. *Applications of the Radon transform, Stratigraphic filtering and Objected-based Stochastic Reservoir Modeling*. PhD thesis, Virginia Tech, 2004.
- R. H. J. M. Otten and L. P. P. P. Van Ginneken. *The Annealing Algorithm*, volume 72 of *Kluwer International Series in Engineering and Computer Science*. Kluwer Academic Publishers, Boston, MA, 1989.
- B. M. Page. The southern Coast Ranges. In W. G. Ernst, editor, *The Geotectonic Development of California*, pages 329–417. Prentice-Hall, Englewood Cliffs, NJ, 1981.
- B. M. Page and D. C. Engebretson. Correlation between the geologic record and the computed plate motions of central California. *Tectonics*, 3:133–155, 1984.
- K. E. Peters, M. H. Pytte, T. D. Elam, and P. Sundararaman. Identification of petroleum systems adjacent to the San Andreas Fault, California, USA. In L. B. Magoon and W. G. Dow, editors, *The Petroleum System from Source to Trap*, AAPG Memoir 60, pages 423–436. AAPG, Tulsa, OK, 1994.
- J. L. Piver. Integration of geologic models and seismic data to characterize interwell heterogeneity of the miocene Temblor formation, Coalinga, California. Master's thesis, Clemson University, 2004.
- RMS. Roxar, Houston, TX, 2002.
- H. R. Schwarz. *Numerical Analysis*. Wiley, New York, 1989.
- J. R. Tague, E. L. Von Dohlen, and G. F. Hollman. Optimizing steamflood performance using 3-D/4-D seismic imaging. *Petroleum Engineer International*, 72(6):29–34, June 1999.

M. T. Taner, F. Koehler, and R. E. Sheriff. Complex seismic trace analysis. *Geophysics*, 44(6):1041–1063, June 1979.